

Discrete Chi-Square Method beats Discrete Fourier Transform and other similar parametric time series analysis methods

Lauri Jetsu

Department of Physics, P.O. Box 64, FI-00014 University of Helsinki, Finland

Contributing authors: lauri.jetsu@helsinki.fi; lauri.jetsu@helsinki.fi;

Abstract

We compare two time series analysis methods, the Discrete Fourier Transform (DFT) and our Discrete Chi-square Method (DCM). DCM is designed for detecting signal(-s) superimposed on an unknown trend. The analytical solution for the non-linear DCM model is an ill-posed problem. We present a computational statistical well-posed solution for this problem. The backbone of DCM is the Gauß-Markov theorem that the least squares fit is the best unbiased estimator for linear regression models. DCM can not fail because this simple time series analysis method computes a massive number of linear least squares fits. Hence, the data spacing, even or uneven, is irrelevant. We use the Fisher-test to identify the best DCM model from all alternative tested DCM models. This best model must also pass our Predictivity-test. Our analyses of simulated complex data sets expose the weaknesses of DFT and the efficiency of DCM. The DFT and DCM are frequency-domain parametric methods. There are many other similar parametric methods. Just like DFT, those other methods suffer from their own particular application limitations. The list of those limitations is long. DCM suffers from none of those limitations. The performance of DCM depends only on the data set size and accuracy. DCM is an ideal forecasting method because the data set time span (ΔT) is irrelevant. It does not matter how long (ΔT) and/or complex the data set is because DCM will inevitably detect the signal(-s) and the trend when the data set size (n) and/or accuracy (σ) become adequate.

Keywords: Computational statistics, Ill-posed problems, Non-linear time series analysis models, Discrete Chi-square Method, Discrete Fourier Transform

1 Introduction

Legendre (1805) formulated the least squares method. Gauß (1809) connected this method to the principles of probability and the normal distribution. A few years later, he showed that the least-squares method gives the best unbiased estimates for the free parameters of linear models, if the zero mean data errors are equal, normally distributed and uncorrelated (Gauß 1821). The extended Gauß-Markov theorem states that the least squares method gives the best estimates for the free parameters of linear models, even if the

data errors do not pass all the above-mentioned criteria (Wooldridge 2010). The Gauß-Markov theorem is the backbone of our DCM. This time series analysis method performs a massive number of linear least squares fits to find the best model for the data.

Hadamard (1902) defined the three conditions for a well-posed problem. The solution for the problem determines these conditions.

C₁ Existence: A solution exists.

C₂ Uniqueness: The solution is unique.

C₃ Stability: Small changes in the input data cause small changes in the solution.

Stability means that the solution behaves predictably as the input varies. In other words, there exists a continuous mapping from the input space to the solution space. If any of these conditions are not satisfied, the problem is classified as ill-posed.

Ill-posed problems arise in many fields of science (Rudin 1976; Tikhonov and Arsenin 1977; Lavrentiev et al. 1986). Typical examples are partial differential equation solutions (Hadamard 1923), nonlinear parameter estimation (Bard 1974) and regularisation of inverse problems (Engl et al. 1996; Vogel 2002). Ill-posed problems are encountered in time series analysis (Berger 2013; Box et al. 2015) because the models for the data are often non-linear (Tong 1990; Tsay and Chen 2018). The unknown free parameters of the model, namely the frequencies, are in the arguments of trigonometric functions representing the signals. This causes non-linearity because the model partial derivatives contain free parameters of the model.

There are numerous techniques for solving the ill-posed problem of detecting one signal superimposed on a trend, especially for evenly spaced data (Cleveland et al. 1990; Shumway and Stoffer 2006; Brockwell and Davis 2009). Kay and Marple (1981) compared many spectral estimating techniques that can detect more than one signal from evenly spaced data. They discussed how the time span of data (ΔT) limits the frequency resolution for detecting many signals and causes leakage that shifts power from one spectral peak to another. The spectral estimating techniques fail if the data are non-stationary. Therefore, trends changing the sample mean and/or variance must be removed before applying spectral estimation (Nerlove 1964). Ghaderpour et al. (2021) presented different techniques for reducing spectral leakage. They also discussed techniques for detecting many signals in unevenly spaced data, if these signals are pure sines.

However, no published solution seems to exist for the more complex data sets, where the signal periods are longer than ΔT and/or these signals are not pure sines. We will show that DCM can find a well-posed computational statistical solution even for such complex data sets. This method can detect an unknown number of periodic signals

superimposed on an unknown aperiodic trend. The noise level can be unknown because the performance of DCM depends only on the sample size (n) and data accuracy (σ). The time span (ΔT) is irrelevant. The data spacing, even or uneven, is also irrelevant.

In this study, we apply one published DFT version (Horne and Baliunas 1986) to analyse artificial simulated unevenly spaced data having equal weights. The performance of this DFT version is compared to the performance of our DCM.

We present the DCM formulation in Section 2.1. Data sets are simulated using the DCM model (Sect. 2.2). The four DFT application limitations are discussed in Section 2.3 (Equations 27-30). DCM and DFT time series analysis of the simulated data sets shows that DCM does not suffer from the DFT application limitations (Sects. 3.1-3.7). We then present the identification of the best DCM model for the data (Sect. 3.8), the DCM significance estimates (Sect. 3.9) and the DCM predictions (Sect. 3.10). Finally, we discuss our results (Sect. 4).

2 Methods

The observations are $y_i = y(t_i) \pm \sigma(t_i)$, where t_i are the observing times and σ_i are the errors ($i = 1, 2, \dots, n$). The time span of data, which is also called the data window, is $\Delta T = t_n - t_1$. The mid point is $t_{\text{mid}} = t_1 + \Delta T/2$. The mean and the standard deviation of all y_i values are denoted with m and s .

2.1 Discrete Chi-square method (DCM)

Jetsu (2020) formulated DCM. The model of this method is

$$g(t) = g(t, K_1, K_2, K_3) = h(t) + p(t), \quad (1)$$

where the integer values K_1 , K_2 and K_3 are called the model orders. The notation $g_{K_1, K_2, K_3}(t)$ is used to specify these orders. The DCM model is a sum of two functions. These functions are the periodic function

$$h(t) = h(t, K_1, K_2) = \sum_{i=1}^{K_1} h_i(t, f_i) \quad (2)$$

$$h_i(t, f_i) = \sum_{j=1}^{K_2} B_{i,j} \cos(2\pi j f_i t) + C_{i,j} \sin(2\pi j f_i t) \quad (3)$$

and the aperiodic function

$$p(t) = p(t, K_3) = \begin{cases} 0, & \text{if } K_3 = -1 \\ \sum_{k=0}^{K_3} p_k(t), & \text{if } K_3 = 0, 1, 2, \dots \end{cases} \quad (4)$$

where

$$p_k(t) = M_k \left[\frac{2(t - t_{\text{mid}})}{\Delta T} \right]^k. \quad (5)$$

For $k > 1$, the $p_k(t)$ function full range is

$$\begin{cases} 2|M_k|, & \text{if } k \text{ is odd} \\ |M_k|, & \text{if } k \text{ is even.} \end{cases} \quad (6)$$

The free parameters of $g(t)$ model are

$$\begin{aligned} \boldsymbol{\beta} &= [\beta_1, \beta_2, \dots, \beta_\eta] \\ &= [B_{1,1}, C_{1,1}, f_1, \dots, B_{K_1, K_2}, C_{K_1, K_2}, f_{K_1}, \\ &\quad M_0, \dots, M_{K_3}]. \end{aligned} \quad (7)$$

The number of free parameters is

$$\eta = K_1 \times (2K_2 + 1) + K_3 + 1. \quad (8)$$

We divide the free parameters $\boldsymbol{\beta}$ into two groups $\boldsymbol{\beta}_I$ and $\boldsymbol{\beta}_{II}$. The first group are the frequencies

$$\boldsymbol{\beta}_I = [f_1, \dots, f_{K_1}]. \quad (9)$$

Due to this group, all free parameters are not eliminated from all partial derivatives $\partial g / \partial \beta_i$. This makes the $g(t)$ model *non-linear*. If the $\boldsymbol{\beta}_I$ frequencies have constant values, the multipliers $2\pi j f_i$ in Equation 3 become constants. In this case, the model becomes *linear* because the partial derivatives $\partial g / \partial \beta_i$ no longer contain any free parameters. The solution for the second group of remaining free parameters

$$\boldsymbol{\beta}_{II} = [B_{1,1} C_{1,1}, \dots, B_{K_1, K_2}, C_{K_1, K_2}, M_0, \dots, M_{K_3}] \quad (10)$$

becomes *unique*. This solution passes the C_1 , C_2 and C_3 conditions of a well-posed problem.

Let us assume that we search for periods between f_{\min} and f_{\max} . The non-linear $g(t)$ model becomes linear, if the tested $\boldsymbol{\beta}_I$ frequencies are fixed to any constant values. The sum $h(t)$ of signals $h_1(t, f_1)$, $h_2(t, f_2) \dots$ and $h_{K_1, f_{K_1}}(t)$ does not depend on the order in which these signals are added. For example, the two signal $K_1 = 2$ model symmetry is $h(t) = h_1(t, f_1) + h_2(t, f_2) = h_1(t, f_2) + h_2(t, f_1)$. Both (f_1, f_2) and (f_2, f_1) combinations give the same value for the $g(t)$ model. Since this symmetry applies to any K_1 number of signals, we compute the linear $g(t)$ models only for all tested frequency combinations

$$f_{\max} \geq f_1 > f_2 > \dots > f_{K_1} \geq f_{\min}. \quad (11)$$

The DCM model residuals

$$\epsilon_i = y(t_i) - g(t_i) = y_i - g_i. \quad (12)$$

give the sum of squared residuals

$$R = \sum_{i=1}^n \epsilon_i^2, \quad (13)$$

and the Chi-square

$$\chi^2 = \sum_{i=1}^n \frac{\epsilon_i^2}{\sigma_i^2}. \quad (14)$$

For every tested $\boldsymbol{\beta}_I = [f_1, f_2, \dots, f_{K_1}]$ frequency combination, the DCM test statistic

$$z = z(f_1, f_2, \dots, f_{K_1}) = \sqrt{R/n} \quad (15)$$

$$z = z(f_1, f_2, \dots, f_{K_1}) = \sqrt{\chi^2/n} \quad (16)$$

is computed from a linear model least squares fit. Equation 15 or Equation 16 is applied for unknown or known σ_i errors, respectively. The value of z is unique.

In the preliminary long search, we test an evenly spaced grid of n_L frequencies between f_{\min} and f_{\max} . This search gives the best frequency candidates $f_{1, \text{mid}}, \dots, f_{K_1, \text{mid}}$.

In the final short search, we test a denser grid of n_S frequencies within an interval

$$[f_{i, \text{mid}} - a, f_{i, \text{mid}} + a], \quad (17)$$

where $i = 1, \dots, K_1$, $a = c(f_{\min} - f_{\max})/2$ and $c = 0.05$.

The total number of all tested long and short search frequency combinations is

$$\binom{n_f}{K_1} = \frac{n_f!}{K_1!(n_f - K_1)!}, \quad (18)$$

where $n_f = n_L$ and $n_f = n_S$, respectively. The even or uneven data spacing is irrelevant because the linear least squares fit result for every tested frequency combination does not depend on this spacing.

The global periodogram minimum

$$z_{\min} = z(f_{1,\text{best}}, f_{2,\text{best}}, \dots, f_{K_1,\text{best}}) \quad (19)$$

is at the tested frequencies $f_{1,\text{best}}, f_{2,\text{best}}, \dots, f_{K_1,\text{best}}$. This tested frequency combination gives the best linear model for the data. The periodogram value z is a scalar, which is computed from K_1 frequency values. It is possible to plot the $K_1 = 2$ two signal periodogram $z(f_1, f_2)$ as a map, where f_1 and f_2 are the coordinates, and $z = z(f_1, f_2)$ is the height. For more than two signals, there is no direct graphical z plot because that requires more than three dimensions. Our solution for this dimensional problem is simple. We plot only the following one-dimensional slices of the full periodogram

$$\begin{aligned} z_1(f_1) &= z(f_1, f_{2,\text{best}}, \dots, f_{K_1,\text{best}}) \\ z_2(f_2) &= z(f_{1,\text{best}}, f_2, f_{3,\text{best}}, \dots, f_{K_1,\text{best}}) \\ z_3(f_3) &= z(f_{1,\text{best}}, f_{2,\text{best}}, f_3, f_{4,\text{best}}, \dots, f_{K_1,\text{best}}) \\ z_4(f_4) &= z(f_{1,\text{best}}, f_{2,\text{best}}, f_{3,\text{best}}, f_4, f_{5,\text{best}}, \dots, f_{K_1,\text{best}}) \\ z_5(f_5) &= z(f_{1,\text{best}}, f_{2,\text{best}}, f_{3,\text{best}}, f_{4,\text{best}}, f_5, \dots, f_{K_1,\text{best}}) \\ z_6(f_6) &= z(f_{1,\text{best}}, f_{2,\text{best}}, f_{3,\text{best}}, f_{4,\text{best}}, f_{5,\text{best}}, f_6). \end{aligned} \quad (20)$$

In the above-mentioned $K_1 = 2$ map, the slice $z_1(f_1)$ would represent the height z at the location $(f_1, f_{2,\text{best}})$ when moving along the straight constant line $f_2 = f_{2,\text{best}}$ that crosses the global minimum z_{\min} (Equation 19) at the coordinate point $(f_{1,\text{best}}, f_{2,\text{best}})$. These one-dimensional periodogram slices (Equation 20) allow us "to see inside" the multi-dimensional structure of the DCM test statistic z (Equations 15 and 16). This kind of visualisation is important in time series analysis (Su and Wu 2024).

The short search gives the best $f_{1,\text{best}}, \dots, f_{K_1,\text{best}}$ frequencies for the data. These frequencies are the *unique* initial values for the first

group of free parameters $\beta_{\text{I,initial}} = [f_{1,\text{best}}, \dots, f_{K_1,\text{best}}]$ (Equation 9). The linear model for these constant $[f_{1,\text{best}}, \dots, f_{K_1,\text{best}}]$ frequencies gives the *unique* initial values for the second group $\beta_{\text{II,initial}}$ of free parameters (Equation 10). The non-linear iteration

$$\beta_{\text{initial}} = [\beta_{\text{I,initial}}, \beta_{\text{II,initial}}] \rightarrow \beta_{\text{final}} \quad (21)$$

gives the final free parameter values β_{final} .

Furlan and Mortarino (2020) emphasise that the analytical error estimates for the non-linear model free parameters can be tricky. They compare different analytical free parameter error estimating methods by using the computational statistical bootstrap technique (Efron and Tibshirani 1986). They conclude that the analytical error estimates become less reliable if the number of free parameters increases. For our non-linear DCM model, we determine the i :th signal parameters

$$\begin{aligned} P_i &= 1/f_i = \text{Period} \\ A_i &= \text{Peak to peak amplitude} \\ t_{i,\text{min},1} &= \text{Deeper primary minimum} \\ t_{i,\text{min},2} &= \text{Secondary minimum (if present)} \\ t_{i,\text{max},1} &= \text{Higher primary maximum} \\ t_{i,\text{max},2} &= \text{Secondary maximum (if present)} \end{aligned}$$

and the trend parameters

$$M_k = \text{Polynomial coefficients.}$$

Of these model parameters, all $P_i = 1/f_i$ and all M_k estimates are among the free parameters β . However, the $A_i, t_{i,\text{min},1}, t_{i,\text{min},2}, t_{i,\text{max},1}$ and $t_{i,\text{max},2}$ model parameters depend on β values. The analytical solutions for these model parameters are simple for pure sines ($K_2 = 1$), but become quite complicated for double waves ($K_2 = 2$). Clearly, the analytical solution for the errors of DCM model parameters would be tedious. The analytical solution for the model error

$$g(t) \pm \sigma_{g(t)} \quad (22)$$

would be practically impossible because the number of DCM model free parameters is large, especially if the data contains many signals. We use the computational statistical bootstrap technique (Efron and Tibshirani 1986) to solve these analytical problems. This approach gives the DCM model parameter error estimates, as well as the $\sigma_{g(t)}$ model error estimates (Equation 22). In our

bootstrap, the tested frequencies are the same as in the short search. We select a random sample ϵ^* from the residuals ϵ of the DCM model (Equation 12). Any ϵ_i value can be chosen to the ϵ^* sample as many times as the random selection happens to favour it. We create numerous *artificial* bootstrap data sets

$$\mathbf{y}^* = \mathbf{g} + \epsilon^*. \quad (23)$$

Each \mathbf{y}^* sample gives *one estimate* for every DCM model parameter value and model $g(t)$ value. For each particular model parameter and each particular $g(t)$, the bootstrap error estimate is the standard deviation of *all estimates* obtained from all \mathbf{y}^* samples.

There are, of course, totally wrong DCM models for the data. For example, DCM can be forced search for too few or too many K_1 signals, or the selected $p(t)$ trend order K_3 can be wrong, as shown in Figures 5-10 by Jetsu (2020). Such DCM models are unstable and we denote them with “UM”, like in Jetsu¹ (2025). These unstable models have three signatures

Intersecting frequencies
 Dispersing amplitudes
 Leaking periods

Intersecting frequencies occur when the signal frequencies in the data are very close to each other. We give the following example of how this instability can arise in the two signal model. If the frequency f_1 approaches the frequency f_2 , both $h_1(t)$ and $h_2(t)$ signals become essentially one and the same signal. The least squares fit fails because it makes no sense to model the same signal twice.

Dispersing amplitudes instability can occur, if the two signal frequencies are too close to each other. The least squares fit finds a model, where two high amplitude signals nearly cancel out each other. The low amplitude signal, the sum of these two high amplitude signals, fits to the data.

There are DCM models where the detected frequency f is outside the tested frequency interval between f_{\min} and f_{\max} . This leaking periods instability may indicate that the chosen tested period range is wrong.

¹Jetsu L. “Do planets cause the sunspot cycle?”, submitted to Scientific Reports. August 13th, 2025.

2.2 Simulated DCM model data samples

We use seven different $g(t)$ models to simulate 21 artificial complex data sets (Sections 3.1-3.7). The time interval of all simulated data sets is $\Delta T = 1$. The n^* simulated time points t_i^* are drawn from a random uniform distribution $U(0, \Delta T, n^*)$. The first and last time point values are then modified to $t_1^* = 0$ and $t_n^* = \Delta T$. Hence, the distance between independent frequencies (Kay and Marple 1981) is always

$$f_0 = 1/\Delta T = 1. \quad (24)$$

The n^* residuals $\epsilon^*(t_i^*)$ of simulated model are drawn from a random normal distribution $N(0, \sigma, n^*)$, where σ is the accuracy of simulated data. The simulated data are

$$\begin{aligned} y^*(t_i^*) &= g(t_i^*) + \epsilon^*(t_i^*) \\ &= h(t_i^*) + p(t_i^*) + \epsilon^*(t_i^*). \end{aligned}$$

The peak to peak amplitudes of all simulated signals is $A = 2$. Our definition for the signal to noise ratio is

$$\text{SN} = (A/2)/\sigma. \quad (25)$$

2.3 Discrete Fourier Transform (DFT)

We search for signals in the simulated data using the DFT version formulated by Horne and Balinas (1986). This method searches for the best pure sine model for the data. The notations for the DFT model are

$$g_{\text{DFT}}(t) = s_{\text{DFT}}(t) + p_{\text{DFT}}(t), \quad (26)$$

where $s_{\text{DFT}}(t)$ is the pure sine signal and $p_{\text{DFT}}(t)$ is the trend. The pure sine signals for the y_i data and the ϵ_i residuals are denoted with $s_{y,\text{DFT}}(t)$ and $s_{\epsilon,\text{DFT}}(t)$, respectively. Our DFT analysis may fail due to four application limitations.

The data sample is “too short” (Kay and Marple 1981)

$$P > \Delta T. \quad (27)$$

Table 1 Model 1: DCM analysis between $P_{\min} = 0.63$ and $P_{\max} = 5.70$. (1) Simulated P_1 , A_1 , $t_{1,\min,1}$, $t_{1,\max,1}$ and M_0 values. (2-4) Detected values for different n and SN combinations. Two lowest lines specify electronic data files and DCM analysis control files.

(1)	(2)	(3)	(4)
	$n = 50$ SN = 10	$n = 50$ SN = 50	$n = 100$ SN = 100
Model 1			
$P_1 = 1.9$	1.58 ± 0.21	1.822 ± 0.042	1.863 ± 0.017
$A_1 = 2.0$	1.64 ± 0.33	1.894 ± 0.072	1.941 ± 0.025
$t_{1,\min,1} = 1.35$	1.20 ± 0.11	1.312 ± 0.021	1.3321 ± 0.0088
$t_{1,\max,1} = 0.40$	0.4098 ± 0.0058	0.4007 ± 0.0013	0.40056 ± 0.00078
$M_0 = 1.0$	1.20 ± 0.18	1.061 ± 0.036	1.030 ± 0.014
Data file	Model1n50SN10.dat	Model1n50SN50.dat	Model1n100SN100.dat
Control file	dcmModel1n50SN10.dat	dcmModel1n50SN50.dat	dcmModel1n100SN100.dat

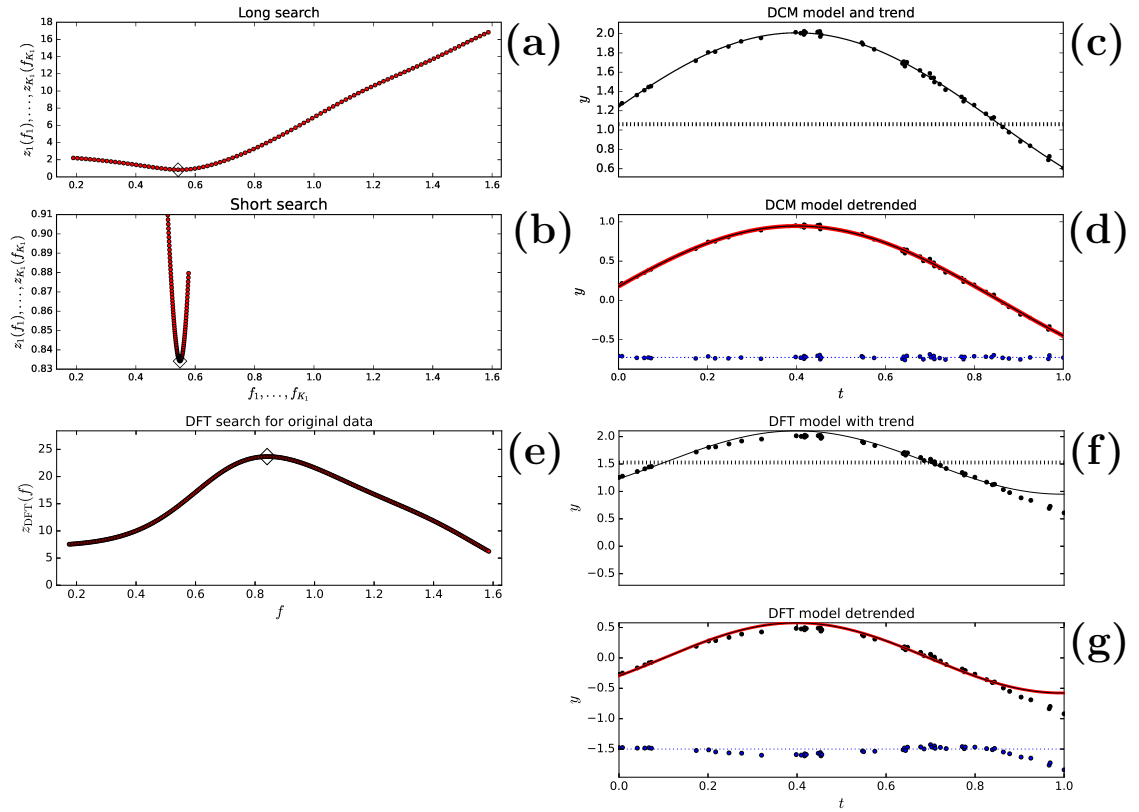


Fig. 1 Model 1 (Table 1: $n = 50$, SN = 50 simulation). (a) DCM long search periodogram $z_1(f_1)$ gives best period at 1.843 (diamond). (b) DCM short search periodogram $z_1(f_1)$ gives best period at 1.822 (diamond). (c) DCM model $g(t)$ (black continuous line), DCM trend $p(t)$ (black dashed line) and data y_i (black dots). (d) DCM model detrended $g(t) - p(t)$ (black continuous line), DCM signal $h_1(t)$ (red thick continuous line), detrended data $y(t_i) - p(t_i)$ (black dots) and DCM model residuals $y(t_i) - g(t_i)$ (blue dots) offset to -0.65 level (blue dotted line). (e) DFT periodogram $z_{DFT}(f)$ gives best period at 1.190 (Diamond). (f) DFT model $g_{DFT}(t)$ (black continuous line), DFT trend $p_{DFT}(t)$ (black dashed line) and data y_i (black dots). (g) DFT model detrended $g_{DFT}(t) - p_{DFT}(t)$ (black continuous line), DFT pure sine $s_{DFT}(t)$ (red thick continuous line), detrended data $y(t_i) - p_{DFT}(t_i)$ (black dots) and DFT model residuals (blue dots) offset to -1.5 level (blue dotted line).

The data contain “a trend” (Nerlove 1964)

$$p_{\text{DFT}}(t) \neq 0. \quad (28)$$

The signal frequencies are “too close” (Kay and Marple 1981).

$$|f_1 - f_2| < f_0 = \Delta T^{-1}. \quad (29)$$

The signals are not “pure sines” (Bretthorst 1988).

$$K_2 \neq 1. \quad (30)$$

The $p_i = p_{\text{DFT}}(t_i)$ trend is first removed from the data $y_i = y(t_i)$ (Nerlove 1964). Then, the technique described by Ghaderpour et al. (2021) is used to detect the pure sine signals. We apply the DFT to the detrended $y_i - p_i$ data. When searching for the second signal, we apply the DFT to the original model residuals $\epsilon_i = y_i - g_{\text{y,DFT}}(t_i)$.

3 Results

We apply DCM and DFT to seven different simulated data sets (Sections 3.1 - 3.7). As we proceed, these data sets become increasingly complex. DCM analysis succeeds for all data sets. DFT analysis fails for every data set.

3.1 Model 1

Our first simulation model is the one signal model

$$g(t) = (A_1/2) \cos \left[\frac{2\pi(t - t_{1,\max,1})}{P_1} \right] + M_0. \quad (31)$$

We give the P_1 , A_1 , $t_{1,\max,1}$ and M_0 values in Table 1 (Column 1). This sample is “too short” (Equation 27) because $P_1 = 1.9\Delta T$. The constant mean level M_0 is unknown (Equation 28). We perform the DCM and DFT time series analysis between $P_{\min} = P_1/3 = 0.63$ and $P_{\max} = 3P_1 = 5.70$.

Model 1 is a DCM model, where $K_1 = 1$, $K_2 = 1$, $K_3 = 0$, $B_{1,1} = (A_1/2) \cos(2\pi f_1 t_{1,\max,1})$ and $C_{1,1} = (A_1/2) \sin(2\pi f_1 t_{1,\max,1})$. We give the DCM analysis results for three samples having different n and SN combinations (Table 1: Columns 2-4). For each sample, this table specifies the electronic data file and the electronic DCM control

file.² The detected P_1 , A_1 , $t_{1,\max,1}$ and M_0 values are correct and accurate even for the combination $n = 50$ and $\text{SN} = 50$. These values become more accurate when n and SN increase.

A graphical presentation of DCM analysis results is shown for Model 1 simulated data sample, where $n = 50$ and $\text{SN} = 50$ (Figures 1a-d). The DCM long search $z_1(f_1)$ periodogram minimum is at $P_1 = 1.843$ (Figure 1a: diamond). The DCM short search periodogram $z_1(f_1)$ gives the best period at $P_1 = 1.822$ (Figure 1b: diamond). The continuous black line denoting the DCM model $g(t)$ fits perfectly to the black dots denoting the data y_i (Figure 1c). The mean $p(t) = M_0 = 1.061 \pm 0.036$ is correct (Figure 1c: dashed black line). The detrended model $g(t) - p(t)$ (black continuous line), the detrended data $y(t_i) - p(t_i)$ (black dots) and the pure sine signal $h_1(t)$ (red thick continuous line) are shown in Figure 1d. Note that the thick continuous red line stays under the thin continuous black line because $h_1(t) = g(t) - p(t)$. The DCM residuals (blue dots) are offset to the level of -0.65 (blue dotted line). These residuals are stable and display no trends.

The DFT detects the wrong period $P_1 = 1.190$ (Figure 1e: Diamond). The DFT mean level estimate $M_0 = 1.527$ is also wrong (Figure 1f: Dashed black line). The black dots denoting the data y_i deviate from the continuous black line denoting the DFT model $g_{\text{DFT}}(t)$. The detrended model $g_{\text{DFT}}(t) - p_{\text{DFT}}(t)$ (continuous black line), the detrended data $y(t_i) - p_{\text{DFT}}(t_i)$ (black dots) and the signal $s_{\text{y,DFT}}(t)$ (continuous thick red line) are shown in Figure 1g. The thin black line covers the thick red line because $s_{\text{y,DFT}}(t) = g_{\text{DFT}}(t) - p_{\text{DFT}}(t)$. The DFT residuals (blue dots) offset to the level of -1.5 (blue dotted line) display obvious trends, especially at the end of analysed sample.

For the simulated data of Model 1, the DCM analysis succeeds, but the DFT analysis fails.

3.2 Model 2

Our next one signal data simulation model is

$$g(t) = (A_1/2) \cos \left[\frac{2\pi(t - t_{1,\max,1})}{P_1} \right] + M_0 + M_1 T + M_2 T^2 \quad (32)$$

²We publish all our data files and all DCM control files in <https://zenodo.org/uploads/17018676>

Table 2 Model 2. DCM analysis between $P_{\min} = 0.63$ and $P_{\max} = 4.70$. Notations as in Table 1.

(1)	(2)	(3)	(4)
	$n = 1\ 000$	$n = 10\ 000$	$n = 10\ 000$
Model 2	SN = 100	SN = 100	SN = 200
$P_1 = 1.9$	1.98 ± 0.34	1.852 ± 0.055	1.933 ± 0.040
$A_1 = 2.0$	2.4 ± 2.8	1.84 ± 0.20	2.13 ± 0.16
$t_{1,\min,1} = 1.35$	1.39 ± 0.17	1.326 ± 0.027	1.367 ± 0.020
$t_{1,\max,1} = 0.40$	0.4015 ± 0.0020	0.40007 ± 0.00072	0.40017 ± 0.00075
$M_0 = 1.0$	0.8 ± 1.4	1.079 ± 0.096	0.937 ± 0.080
$M_1 = 0.25$	0.29 ± 0.21	0.229 ± 0.026	0.266 ± 0.020
$M_2 = 0.50$	0.62 ± 0.52	0.451 ± 0.064	0.540 ± 0.049
Data file	Model12n1000SN100.dat	Model12n10000SN100.dat	Model12n10000SN200.dat
Control file	dcmModel12n1000SN100.dat	dcmModel12n10000SN100.dat	dcmModel12n10000SN200.dat

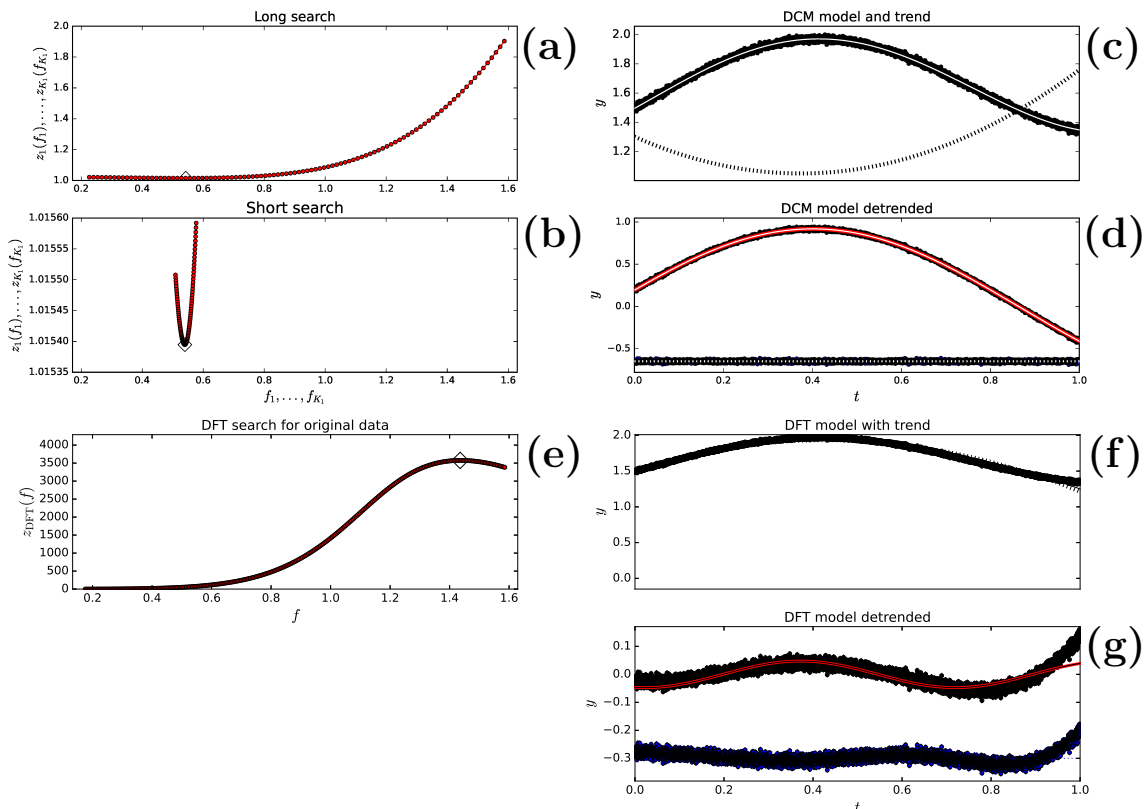


Fig. 2 Model 2 (Table 2: $n = 10\ 000$, SN = 100 simulation). (c) Colour of $g(t)$ line has been changed from black to white. (d) Colour of $g(t)$ line has been changed from black to white. Colour of offset level -0.3 dotted line has been changed from blue to white. Locations of best periods (diamonds) are explained in text (Section 3.2). Otherwise, notations are as in Figure 1.

where $T = [2(t - t_{\text{mid}})]/\Delta T$. We give the P_1 , A_1 , $t_{1,\max,1}$, M_0 , M_1 and M_2 values in Table 2. As a DCM model, the orders of Model 2 are $K_1 = 1$, $K_2 = 1$ and $K_3 = 2$. The simulated data sample is “too short” because the period P_1 is $1.9 \times \Delta T$ (Equation 27). The parabolic trend

$p(t)$ is unknown (Equation 28). Again, we use the DCM and DFT time series analysis methods to search for periods between $P_{\min} = P_1/3 = 0.63$ and $P_{\max} = 3P_1 = 4.70$.

The DCM analysis results are given in Table 2. These results are not very accurate for the

Table 3 Model 3. DCM analysis between $P_{\min} = 0.053$ and $P_{\max} = 0.480$. Notations as in Table 1.

(1)	(2)	(3)	(4)
Model 3	$n = 50$ SN = 10	$n = 50$ SN = 50	$n = 100$ SN = 100
$P_1 = 0.16$	0.15898 ± 0.00068	0.15989 ± 0.00014	0.159950 ± 0.000077
$A_1 = 2.0$	1.85 ± 0.10	1.987 ± 0.036	1.994 ± 0.015
$t_{1,\min,1} = 0.11$	0.1122 ± 0.0020	0.11080 ± 0.00088	0.11004 ± 0.00030
$t_{1,\max,1} = 0.03$	0.0328 ± 0.0022	0.03086 ± 0.00094	0.03007 ± 0.00033
$P_2 = 0.17$	0.17025 ± 0.00066	0.17018 ± 0.00024	0.16996 ± 0.00080
$A_2 = 2.0$	2.001 ± 0.090	1.962 ± 0.046	2.002 ± 0.012
$t_{2,\min,1} = 0.135$	0.1312 ± 0.0022	0.13461 ± 0.00087	0.13495 ± 0.00031
$t_{2,\max,1} = 0.05$	0.0461 ± 0.0024	0.04952 ± 0.00099	0.04997 ± 0.00038
$M_0 = 1.0$	0.996 ± 0.011	0.9985 ± 0.0032	0.9995 ± 0.0012
Data file	Model13n50SN10.dat	Model13n50SN50.dat	Model13n100SN100.dat
Control file	dcmMode13n50SN10.dat	dcmMode13n50SN50.dat	dcmMode13n100SN100.dat

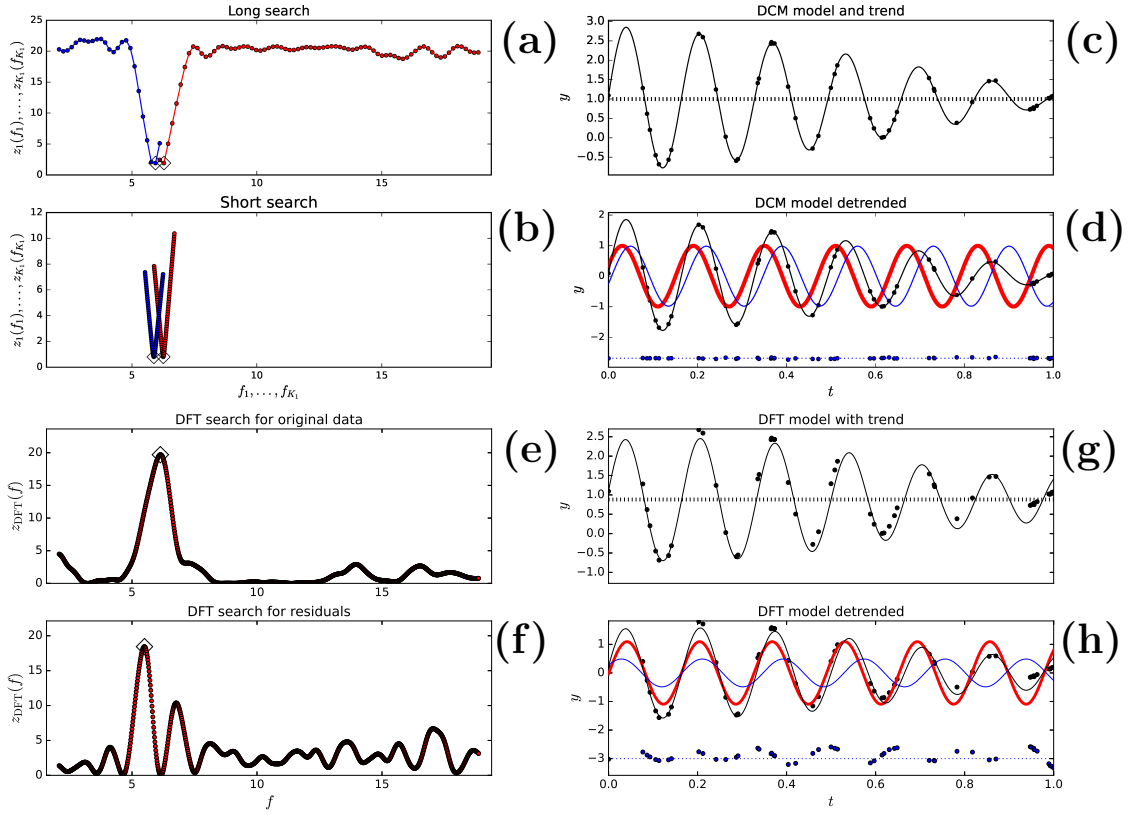


Fig. 3 Model 3 (Table 3: $n = 50$, SN = 50 simulation). (a) DCM long search periodograms $z_1(f_1)$ (red) and $z_2(f)$ (blue) give best periods at 0.160 and 0.168 (diamonds). (b) DCM short search periodograms $z_1(f_1)$ (red) and $z_2(f)$ (blue) give best periods at 0.160 and 0.170 (diamonds). (c) DCM model $g(t)$ (black continuous line), DCM trend $p(t)$ (black dashed line) and data y_i (black dots). (d) DCM model detrended $g(t) - p(t)$ (black continuous line), DCM signal $h_1(t)$ (red thick continuous line), DCM signal $h_2(t)$ (blue continuous thin line), detrended data $y(t_i) - p(t_i)$ (black dots) and DCM model residuals $y(t_i) - g(t_i)$ (blue dots) offset to -3.0 level (blue dotted line) (e) DFT periodogram $z_{\text{DFT}}(f)$ for the original data gives best period at 0.163 (diamond). (f) DFT periodogram $z_{\text{DFT}}(f)$ for the sine model residuals gives best period at 0.182 (diamond). (g) DFT model $g_{\text{DFT}}(t)$ (black continuous line), DFT trend $p_{\text{DFT}}(t)$ (black dashed line) and data y_i (black dots). (h) DFT model detrended $g_{\text{DFT}}(t) - p_{\text{DFT}}(t)$ (black continuous line), DFT pure sine model for original data $s_{y,\text{DFT}}(t)$ (red thick continuous line), DFT pure sine model for first residuals $s_{e,\text{DFT}}(t)$ (blue continuous thin line), detrended data $y(t_i) - p_{\text{DFT}}(t_i)$ (black dots) and DFT model residuals (blue dots) offset to -3.0 level (blue dotted line).

Table 4 Model 4. DCM analysis between $P_{\min} = 0.053$ and $P_{\max} = 0.480$. Notations as in Table 1.

(1)	(2)	(3)	(4)
Model 4	$n = 50$ SN = 10	$n = 50$ SN = 50	$n = 100$ SN = 100
$P_1 = 0.16$	0.1606 ± 0.0084	0.15982 ± 0.00023	0.16001 ± 0.000058
$A_1 = 2.0$	1.97 ± 0.15	1.958 ± 0.051	2.012 ± 0.014
$t_{1,\min,1} = 0.11$	0.1134 ± 0.0036	0.11059 ± 0.00088	0.10977 ± 0.00033
$t_{1,\max,1} = 0.03$	0.0331 ± 0.0040	0.03068 ± 0.00097	0.02976 ± 0.00035
$P_2 = 0.17$	0.1744 ± 0.0012	0.17009 ± 0.00026	0.169958 ± 0.000092
$A_2 = 2.0$	1.74 ± 0.17	1.982 ± 0.044	2.018 ± 0.017
$t_{2,\min,1} = 0.135$	0.1321 ± 0.0044	0.1342 ± 0.0011	0.13528 ± 0.00042
$t_{2,\max,1} = 0.05$	0.0460 ± 0.0048	0.0492 ± 0.0012	0.05031 ± 0.00034
$M_0 = 1.0$	1.015 ± 0.024	0.9997 ± 0.0030	1.0012 ± 0.0016
$M_1 = 0.25$	0.219 ± 0.023	0.2565 ± 0.0066	0.2495 ± 0.0019
$M_2 = 0.5$	0.485 ± 0.050	0.511 ± 0.011	0.4983 ± 0.0033
Data file	Model14n50SN10.dat	Model14n50SN50.dat	Model14n100SN100.dat
Control file	dcmModel14n50SN10.dat	dcmModel14n50SN50.dat	dcmModel14n100SN100.dat

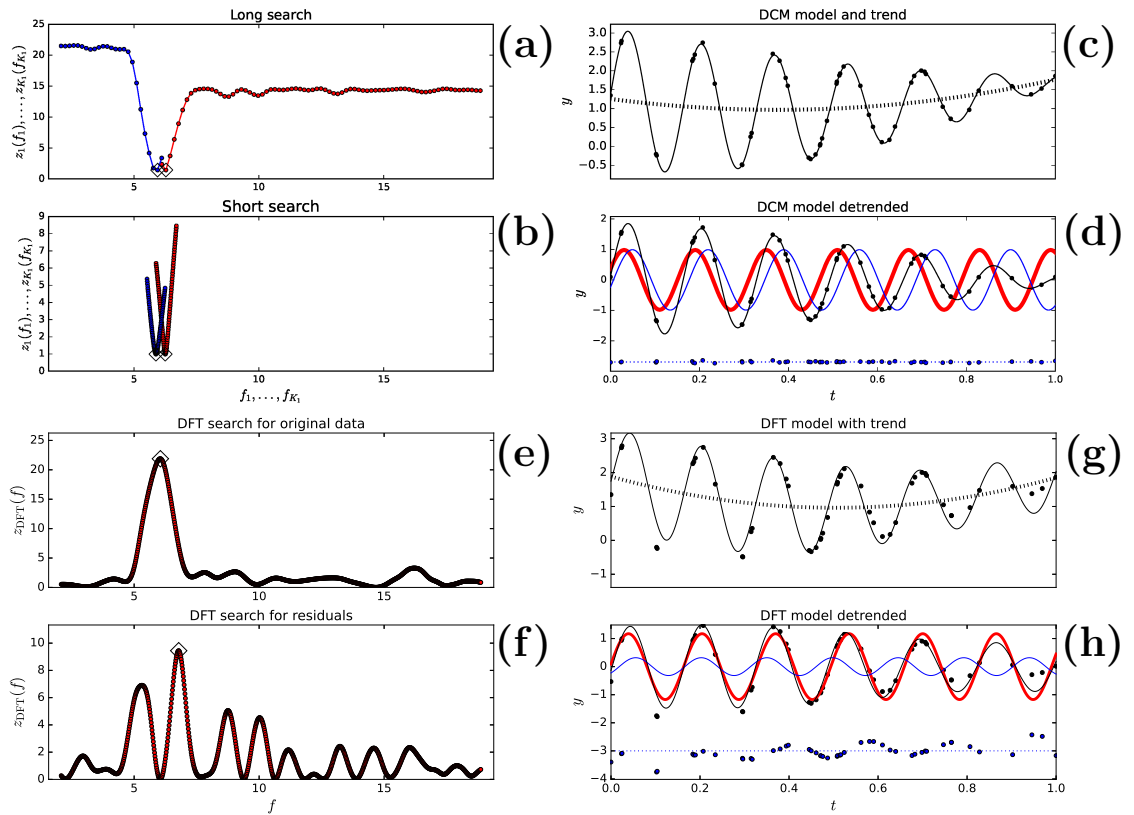


Fig. 4 Model 4 (Table 4: $n = 50$, SN = 50 simulation). Notations as in Figure 3. Best periods (diamonds) are explained in Section 3.4.

$n = 100$ and SN = 100 combination, but they definitely improve for larger n and SN values. For Model 2, the DCM analysis results are illustrated

for the $n = 10\,000$ and SN = 100 combination (Figures 2a-d). The DCM long search $z_1(f_1)$ periodogram minimum is at $P_1 = 1.843$ (Figure 2a: diamond). The DCM short search gives the

value $P_1 = 1.852$ (Figure 2b: diamond). The DCM model $g(t)$ is so good that its continuous black line is totally covered by the black dots representing the y_i data (Figure 2c). Therefore, the colour of this $g(t)$ line has been changed from black to white. The results for the parabolic trend coefficients $M_0 = 1.079 \pm 0.096$, $M_1 = 0.229 \pm 0.026$ and $M_2 = 0.451 \pm 0.064$ of the dashed black $p(t)$ line are correct. In Figure 1d, the white continuous line shows the detrended model $g(t) - p(t)$. The black dots show the detrended data $y(t_i) - p(t_i)$ and the red thick continuous line shows the pure sine signal $h_1(t)$. Note that the red thick line is under the white thin line because $h_1(t) = g(t) - p(t)$. The DCM residuals (blue dots) are offset to the level of -0.65. The colour of dotted line, which denotes this offset level, has been changed from blue to white. The distribution of these DCM model residuals is stable, as expected for a random normal distribution.

The wrong period $P_1 = 0.697$ is detected by DFT (Figure 2e: Diamond). The DFT estimates for the trend $p(t)$ coefficients, $M_0 = 1.92$, $M_1 = -0.15$ and $M_2 = -0.56$ are also wrong (Figure 2f: dashed black line). The data y_i (black dots) deviate from the DFT model $g_{\text{DFT}}(t)$ (black continuous line), especially in the end of the sample (Figure 2g). For the detrended DFT model, the thin black line covers the thick red line because $s_{y,\text{DFT}}(t) = g_{\text{DFT}}(t) - p_{\text{DFT}}(t)$ (Figure 2g). The $s_{y,\text{DFT}}(t)$ sine curve peak to peak amplitude is far below the correct $A_1 = 2.0$ value. The DFT residuals (blue dots) are offset to the level of -1.5 (blue dotted line). The trends of these residuals confirm that the DFT analysis fails.

Only DCM (not DFT) succeeds in the analysis of Model 2 simulated data.

3.3 Model 3

Our third data simulation model is the two signal model

$$g(t) = (A_1/2) \cos \left[\frac{2\pi(t - t_{1,\text{max},1})}{P_1} \right] + (A_2/2) \cos \left[\frac{2\pi(t - t_{2,\text{max},1})}{P_2} \right] + M_0. \quad (33)$$

We give the $P_1, P_2, A_1, A_2, t_{1,\text{max},1}, t_{2,\text{max},1}$ and M_0 values in Table 3 (Column 1). The DCM orders of Model 3 are $K_1 = 2, K_2 = 1$ and

$K_3 = 0$. The simulated data sample is not “too short” (Equation 27) because $P_1 < P_2 < \Delta T$. The $p(t)$ trend mean level M_0 is unknown (Equation 28). The two frequencies are “too close” because $\Delta f = f_1 - f_2 = f_0/2.72$ (Equation 29). We apply the DCM and DFT time series analyses to search for periods between $P_{\text{min}} = P_1/3 = 0.053$ and $P_{\text{max}} = 3P_1 = 0.480$.

The DCM analysis results for different n and SN combinations are given in Table 3 (Columns 2-4). The results are surprisingly accurate even for the small $n = 50$ sample having a low SN = 10. The DCM results for Model 3 are illustrated in Figures 1a-d ($n = 50$ and SN = 50 combination). The DCM long search $z_1(f_1)$ periodogram (red) and $z_2(f)$ periodogram (blue) minima are at the best periods $P_1 = 0.159$ and $P_2 = 0.168$ (Figure 3a: diamonds). The DCM short search gives $P_1 = 0.160$ and $P_2 = 0.170$ (Figure 3b: diamonds). The black continuous DCM model $g(t)$ curve crosses through the black dots of y_i data (Figure 1c). The result $M_0 = 0.9985 \pm 0.0032$ for the dashed black $p(t)$ trend line is correct. Our Figure 3d shows the detrended DCM model $g(t) - p(t)$ (black continuous line), the detrended data $y(t_i) - p(t_i)$ (black dots), the pure sine signal $h_1(t)$ (red thick continuous line) and the pure sine signal $h_2(t)$ (blue thin continuous line). The DCM residuals (blue dots) are offset to the level of -3.0 (blue dotted line). These residuals are small and their level is stable.

The DFT detects the wrong period $P_1 = 1.163$ for the original data (Figure 3e: diamond). This is an expected result because the detected period should be close to $(P_1 + P_2)/2$ when the peak to peak amplitudes of the simulated data, $A_1 = A_2$, are equal (Jetsu 2025). The two DFT periodogram $z_{\text{DFT}}(f)$ peaks at frequencies $1/P_1$ and $1/P_2$ overlap and merge into one peak. The period $P_2 = 0.182$ detected for the residuals is also wrong (Figure 3f: diamond). The DFT trend $p_{\text{PDF}}(t)$ estimate $M_0 = 0.880$ fails (Figure 3f: dashed black line). The black dots y_i show minor deviations from the continuous black DFT model $g_{\text{DFT}}(t)$ line (Figure 3g). The detrended model $g_{\text{DFT}}(t) - p_{\text{DFT}}(t)$ (continuous black line), the detrended data $y(t_i) - p_{\text{DFT}}(t_i)$ (black dots), the pure sine signal $s_{y,\text{DFT}}(t)$ for the data (continuous thick red line) and the pure sine signal $s_{\epsilon,\text{DFT}}(t)$ for the residuals (continuous blue thin line) are shown in Figure 3h. Note that the $s_{y,\text{DFT}}(t)$ and

$s_{\epsilon, \text{DFT}}(t)$ signal amplitudes are far from equal. The DFT residuals (blue dots) offset to the level of -3.0 (blue dotted line) are not stable.

The DCM analysis of Model 3 simulated data succeeds, but the DFT analysis does not.

3.4 Model 4

The next data simulation model is

$$g(t) = (A_1/2) \cos \left[\frac{2\pi(t - t_{1, \max, 1})}{P_1} \right] + (A_2/2) \cos \left[\frac{2\pi(t - t_{2, \max, 1})}{P_2} \right] + M_0 + M_1 T + M_2 T^2, \quad (34)$$

where $T = [2(t - t_{\text{mid}})]/\Delta T$. In this model, two signals are superimposed on an unknown parabolic trend. The P_1 , P_2 , A_1, A_2 , $t_{1, \max, 1}$, $t_{2, \max, 1}$, M_0 , M_1 and M_2 values are given in Table 4. This simulated sample is not “too short” (Equation 27). The polynomial trend $p(t)$ is unknown (Equation 28). The $\Delta f = f_1 - f_2 = f_0/2.72$ difference means that the frequencies are “too close” (Equation 29). The DCM and DFT time series analysis methods are used to search for periods between $P_{\min} = P_1/3 = 0.053$ and $P_{\max} = 3P_1 = 0.480$.

Model 4 is a DCM model having orders $K_1 = 2$, $K_2 = 1$ and $K_3 = 2$. Our DCM analysis results for different n and SN combinations are given in Table 4 (Columns 2-4). The DCM detects the correct P_1 , P_2 , A_1 , A_2 , $t_{\max, 1}$, $t_{\max, 2}$, M_0 , M_1 and M_2 values even for the lowest $n = 50$ and SN = 10 combination. Our Figures 4a-d illustrate the DCM analysis results for one sample of simulated data (Model 4: $n = 50$ and SN = 50). The DCM long search best periods are at $P_1 = 0.159$ and $P_2 = 0.168$ (Figure 4a: diamonds). The DCM short search values are $P_1 = 0.160$ and $P_2 = 0.170$ (Figure 4b: diamonds). The continuous DCM model $g(t)$ black line crosses through all black dots representing the y_i data (Figure 4c). The DCM detects the correct polynomial trend $p(t)$ coefficients $M_0 = 0.9997 \pm 0.0030$, $M_1 = 0.2565 \pm 0.0066$ and $M_2 = 0.511 \pm 0.011$ (Figure 4c: dashed black line). The detrended DCM model $g(t) - p(t)$ (black continuous line), the detrended data $y(t_i) - p(t_i)$ (black dots), the pure sine signal $h_1(t)$ (red thick continuous line) and the pure sine signal $h_2(t)$ (blue thin continuous line) are shown

in Figure 4d. The DCM residuals (blue dots) offset to the level of -3.0 show no trends and are extremely stable.

Since the peak to peak amplitudes of the simulated data signals are equal, $A_1 = A_2$, the expected result for the DFT analysis of original data is $(P_1 + P_2)/2$, where P_1 and P_2 are the simulated signal periods (Jetsu 2025). The DFT detects this expected wrong period $P_1 = 1.165$ for the original data (Figure 4e: diamond). A wrong period $P_2 = 0.147$ is also detected for the residuals (Figure 4f: diamond). The DFT estimate $M_0 = 0.962$ for the $p(t)$ trend is close to the correct value $M_0 = 1$, but the $M_1 = -0.017$ and $M_2 = 0.903$ estimates are wrong (Figure 4g: dashed black line). The continuous black DFT model $g_{\text{DFT}}(t)$ line deviates from the black dots of data y_i , especially in the beginning and end of the sample. In our Figure 4h, the black dots are the detrended data $y(t_i) - p_{\text{DFT}}(t_i)$ and the continuous black line is the detrended DFT model $g_{\text{DFT}}(t) - p_{\text{DFT}}(t)$. The continuous thick red line is the pure sine signal $s_{y, \text{DFT}}(t)$ for the original data and the continuous thinner blue line is the pure sine signal $s_{\epsilon, \text{DFT}}(t)$ for the residuals. The $s_{\epsilon, \text{DFT}}(t)$ signal amplitude is far below the simulated correct value $A_2 = 2.0$. The blue dots representing the DFT model residuals are offset to the level of -3.0 and show clear trends.

Our Model 4 simulated data analysis succeeds for the DCM and fails for the DFT.

3.5 Model 5

The mathematical equation

$$g(t) = (A_1/2) \cos \left[\frac{2\pi(t - t_{1, \max, 1})}{P_1} \right] + (A_2/2) \cos \left[\frac{2\pi(t - t_{2, \max, 1})}{P_2} \right] + M_0 + M_1 T + M_2 T^2 \quad (35)$$

for our fifth model for simulated data is the same for Model 4 (Equation 34). However, this new Model 5 differs from the earlier Model 4 because we use totally different P_1 , P_2 , A_1, A_2 , $t_{1, \max, 1}$, $t_{2, \max, 1}$, M_0 , M_1 and M_2 values (Table 5, Column 1). The simulated data sample is “too short” for both P_1 and P_2 periods (Equation 27). There is “a trend” $p(t)$ (Equation 28). The signal frequencies f_1 and f_2 are “too close” (Equation 29). The three

Table 5 Model 5. DCM analysis between $P_{\min} = 0.47$ and $P_{\max} = 4.20$. Notations as in Table 1.

(1)	(2)	(3)	(4)
	$n = 10\ 000$ SN = 1 000	$n = 10\ 000$ SN = 10 000	$n = 100\ 000$ SN = 10 000
Model 5			
$P_1 = 1.4$	1.404 ± 0.046	1.393 ± 0.014	1.4019 ± 0.0035
$A_1 = 2.0$	2.27 ± 0.45	1.97 ± 0.13	1.994 ± 0.029
$t_{1,\min,1} = 1.1$	1.129 ± 0.023	1.1030 ± 0.0028	1.09766 ± 0.00082
$t_{1,\max,1} = 0.4$	0.4267 ± 0.0012	0.4066 ± 0.0059	0.3967 ± 0.0020
$P_2 = 1.9$	5.24 ± 0.83	2.023 ± 0.094	1.854 ± 0.023
$A_2 = 2.0$	5 ± 24	2.35 ± 0.34	1.918 ± 0.074
$t_{2,\min,1} = 1.55$	3.23 ± 0.50	1.599 ± 0.030	1.5292 ± 0.0066
$t_{2,\max,1} = 0.6$	0.61 ± 0.34	0.587 ± 0.030	0.6024 ± 0.0064
$M_0 = 1.0$	-2 ± 12	0.81 ± 0.16	1.055 ± 0.035
$M_1 = 0.25$	-1.27 ± 0.53	0.230 ± 0.013	0.2590 ± 0.0029
$M_2 = 0.5$	3.8 ± 1.8	0.596 ± 0.084	0.470 ± 0.020
Data file	Model15n10000SN1000.dat	Model15n10000SN10000.dat	Model15n100000SN10000.dat
Control file	dcmModel15n10000SN1000.dat	dcmModel15n10000SN10000.dat	dcmModel15n100000SN10000.dat

Table 6 Model 6. DCM analysis between $P_{\min} = 0.053$ and $P_{\max} = 0.480$. Notations as in Table 1.

(1)	(2)	(3)	(4)
	$n = 50$ SN = 10	$n = 50$ SN = 50	$n = 100$ SN = 100
Model 6			
$P_1 = 0.16$	0.15966 ± 0.00020	0.160022 ± 0.000021	0.160024 ± 0.000019
$A_1 = 2.0$	1.983 ± 0.041	2.0031 ± 0.0086	2.0013 ± 0.0032
$t_{1,\min,1} = 0.0979$	0.09868 ± 0.00057	0.097933 ± 0.000096	0.097934 ± 0.000079
$t_{1,\min,2} = 0.0225$	0.02283 ± 0.00070	0.022563 ± 0.000077	0.022403 ± 0.000071
$t_{1,\max,1} = 0.1421$	0.14241 ± 0.00064	0.142099 ± 0.000079	0.142100 ± 0.000077
$t_{1,\max,2} = 0.0575$	0.05827 ± 0.00057	0.05761 ± 0.00011	0.057448 ± 0.000074
$M_0 = 0$	0.003 ± 0.012	-0.0055 ± 0.0026	0.00176 ± 0.00088
Data file	Model16n50SN10.dat	Model16n50SN50.dat	Model16n100SN100.dat
Control file	dcmModel16n50SN10.dat	dcmModel16n50SN50.dat	dcmModel16n100SN100.dat

main reasons that can cause the failure of DFT analysis are present. We perform the DCM and DFT time series analysis between $P_{\min} = P_1/3 = 0.47$ and $P_{\max} = 3P_1 = 4.20$.

Model 5 has DCM orders $K_1 = 2$, $K_2 = 1$ and $K_3 = 2$. We give the DCM analysis results for different n and SN combinations in Table 5 (Columns 2-4). The DCM fails to detect the correct P_1 , P_2 , ..., M_1 and M_2 values for the the lowest $n = 10\ 000$ and SN = 1 000 combination (Table 5, Column 2). This shows that the DCM can fail, just like any other time series analysis method, if the quality of data is too low. The DCM results for higher n and SN combinations are correct (Table 5, Columns 3-4).

We show the DCM analysis results for one sample of Model 5 simulated data (Figures 5a-d: $n = 10\ 000$ and SN = 10 000). The long and short DCM searches give $P_1 = 1.407$ and $P_2 = 1.917$ (Figure 5a: diamonds), and $P_1 = 1.393$ and $P_2 = 2.024$ (Figure 5b: Diamonds). The continuous line

denoting the model $g(t)$ is totally covered by the black dots of y_i data (Figure 5c). Therefore, we use white colour to highlight this DCM model $g(t)$ line. The detected polynomial trend $p(t)$ coefficients $M_0 = 0.81 \pm 0.16$, $M_1 = 0.230 \pm 0.013$ and $M_2 = 0.596 \pm 0.084$ are correct (Figure 5c: dashed black line). We show the detrended DCM model $g(t) - p(t)$ (white continuous line), the detrended data $y(t_i) - p(t_i)$ (black dots), the signal $h_1(t)$ (red thick continuous line) and the signal $h_2(t)$ (blue thin continuous line) in Figure 5d. The DCM residuals (blue dots) are offset to the level of -1.5. These blue dots appear black because there are 10 000 of them. For obvious reasons, the -1.5 level of these residuals is highlighted by a white dotted line. The DCM model residuals are stable and show no trends.

The DFT detects the wrong periods for the original data (Figure 5e: diamond at $P_1 = 0.592$) and for the residuals (Figure 5f: diamond at $P_2 = 1.012$). The DFT estimates for the $p(t)$ trend,

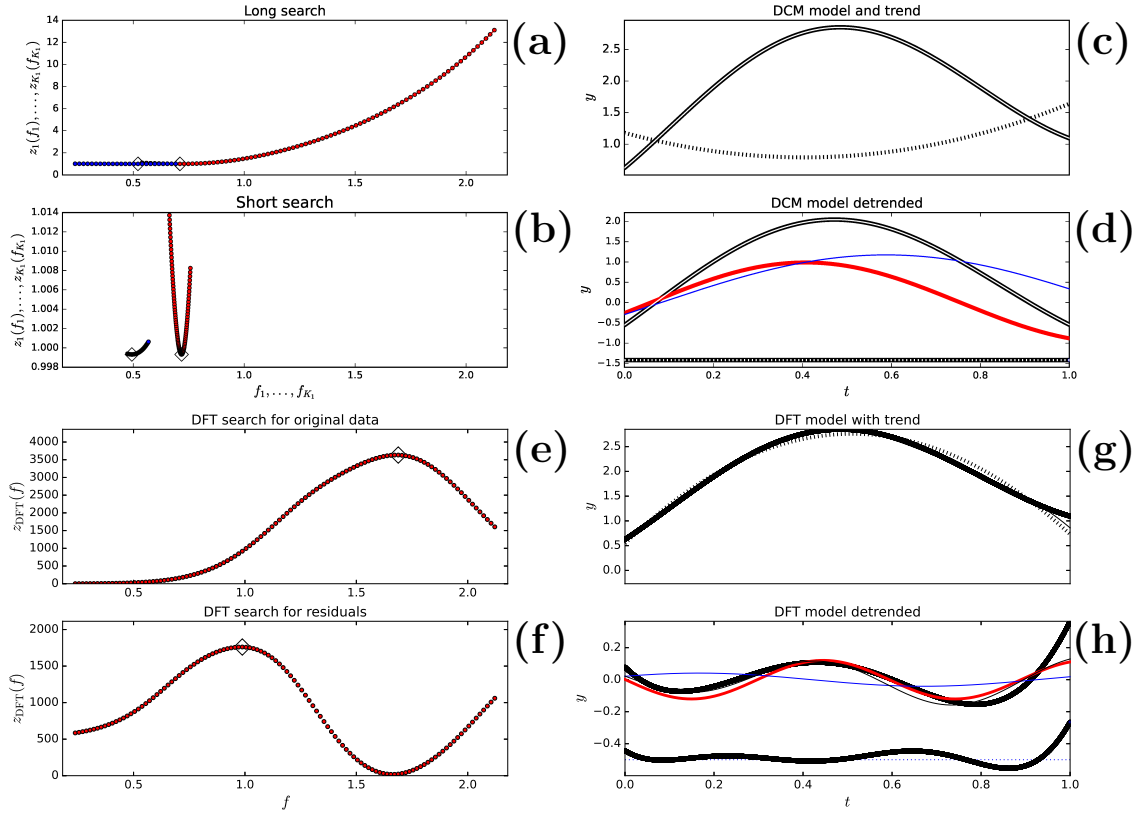


Fig. 5 Model 5 (Table 5: $n = 10\,000$, $\text{SN} = 10\,000$ simulation). Notations as in Figure 3. Best periods (diamonds) are explained in Section 3.5.

Table 7 Model 7. DCM analysis between $P_{\min} = 0.4$ and $P_{\max} = 3.6$. Notations as in Table 1.

(1)	(2) $n = 100$ $\text{SN} = 5\,000\,000$	(3) $n = 1\,000$ $\text{SN} = 1\,000\,000$	(4) $n = 10\,000$ $\text{SN} = 1\,000\,000$
Model 7			
$P_1 = 1.2$	1.19917 ± 0.00070	1.20000 ± 0.00063	1.20000 ± 0.00024
$A_1 = 2.0$	2.20 ± 0.20	1.94 ± 0.14	1.990 ± 0.057
$t_{1,\min,1} = 0.6892$	0.6835 ± 0.0050	0.6900 ± 0.0043	0.6888 ± 0.0019
$t_{1,\min,2} = 0.1134$	0.1235 ± 0.0098	0.1160 ± 0.0067	0.1128 ± 0.0026
$t_{1,\max,1} = 1.0195$	1.0253 ± 0.0052	1.0176 ± 0.0039	1.0188 ± 0.0018
$t_{1,\max,2} = 0.3779$	0.3705 ± 0.0082	0.3804 ± 0.0050	0.3780 ± 0.0020
$P_2 = 1.4$	1.4050 ± 0.0048	1.3986 ± 0.00034	1.3997 ± 0.0014
$A_2 = 2.0$	1.871 ± 0.098	2.049 ± 0.095	2.009 ± 0.040
$t_{2,\min,1} = 0.9262$	0.938 ± 0.012	0.9231 ± 0.0090	0.9252 ± 0.0036
$t_{2,\min,2} = 0.2766$	0.260 ± 0.016	0.281 ± 0.012	0.2771 ± 0.0046
$t_{2,\max,1} = 1.3109$	1.3165 ± 0.0049	1.3105 ± 0.0039	1.3101 ± 0.0014
$t_{2,\max,2} = 0.5864$	0.5817 ± 0.0037	0.5860 ± 0.0042	0.5865 ± 0.0015
$M_0 = 1.0$	0.950 ± 0.050	1.011 ± 0.035	1.002 ± 0.013
$M_1 = 0.25$	0.2447 ± 0.0067	0.2548 ± 0.0039	0.2509 ± 0.0018
$M_2 = 0.5$	0.551 ± 0.050	0.488 ± 0.035	0.498 ± 0.014
Data file	Model7n100SN5000000.dat	Model7n1000SN1000000.dat	Model7n10000SN1000000.dat
Control file	dcmModel7n100SN5000000.dat	dcmModel7n1000SN1000000.dat	dcmModel7n10000SN1000000.dat

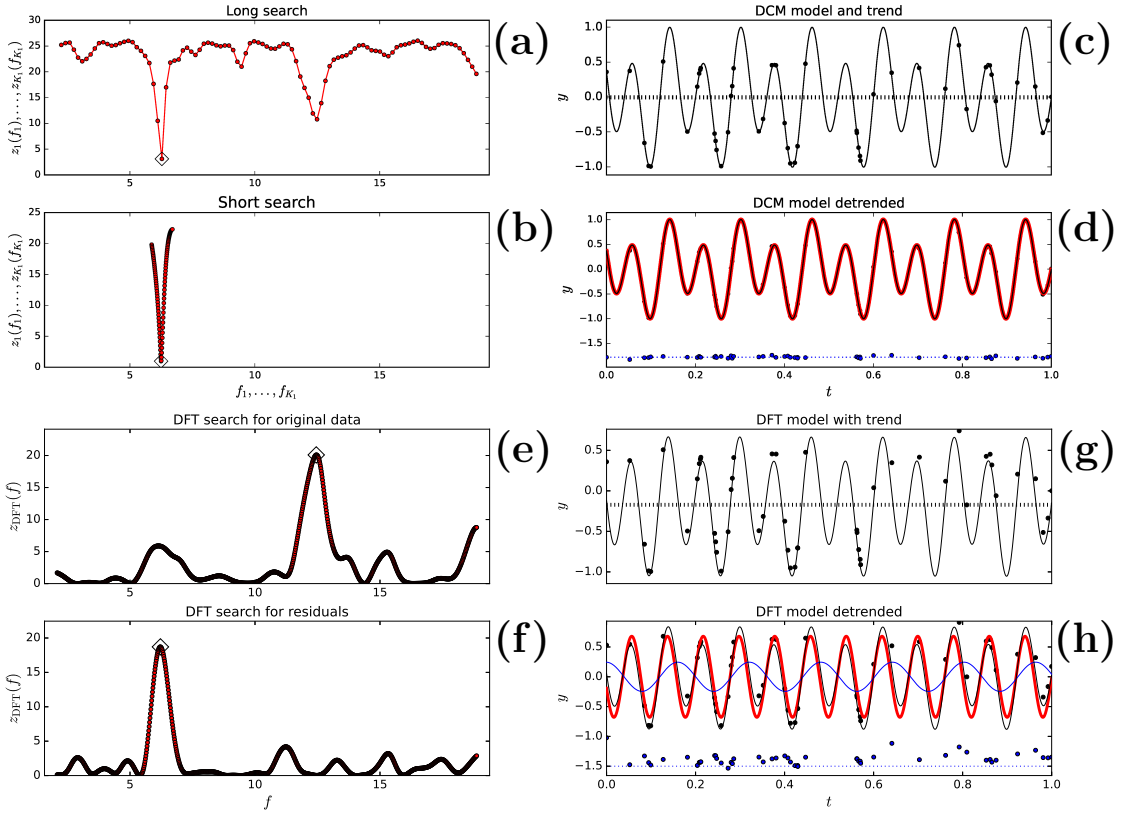


Fig. 6 Model 6 (Table 6: $n = 50$, SN = 50 simulation). Notations as in Figure 3. Best periods (diamonds) are explained in Section 3.6.

$M_0 = 2.758$, $M_1 = 0.091$ and $M_2 = -2.120$, are also wrong (Figure 5g: dashed black line). The DFT model $g_{\text{DFT}}(t)$ black continuous line deviates from the black dots of data y_i , especially in the end of the simulated data sample. The black dots denoting the detrended data $y(t_i) - p_{\text{DFT}}(t_i)$ and the continuous black line denoting the detrended DFT model $g_{\text{DFT}}(t) - p_{\text{DFT}}(t)$ are shown in Figure 5h. The DFT model $g_{\text{DFT}}(t)$ gives very low amplitudes for the pure sine signal $s_{y,\text{DFT}}(t)$ (continuous thick red line) and pure sine signal $s_{\epsilon,\text{DFT}}(t)$ (continuous thinner blue line). These amplitudes are far below the correct simulated values $A_1 = A_2 = 2$. The offset level for the DFT model residuals (blue dots) is -0.5. These residuals show strong trends.

The DCM analysis succeeds for Model 5 simulated data, but the DFT analysis fails.

3.6 Model 6

Our sixth data simulation model is

$$g(t) = c_1 \cos \left[\frac{2\pi t}{P_1} \right] + c_2 \cos \left[\frac{4\pi(t - c_3)}{P_1} \right] + M_0, \quad (36)$$

where $P = 0.16$ and $M_0 = 0$. The coefficients $c_1 = 0.3655$, $c_2 = 0.7310$ and $c_3 = 0.3000$ determine the A_1 , $t_{1,\min,1}$, $t_{1,\min,2}$, $t_{1,\max,1}$ and $t_{1,\max,2}$ values given in Table 6 (Column 1). This simulated data sample is not “too short” because $P_1 < \Delta T$ (Equation 27). There is no trend because $p(t) = M_0 = 0$ (Equation 28). These simulated data contain only one signal (Equation 29). However, this simulation Model 6 is not a $K_2 = 1$ pure sine model (Equation 30). This double wave simulation model has two unequal minima and maxima. Its DCM orders are $K_1 = 1$, $K_2 = 2$

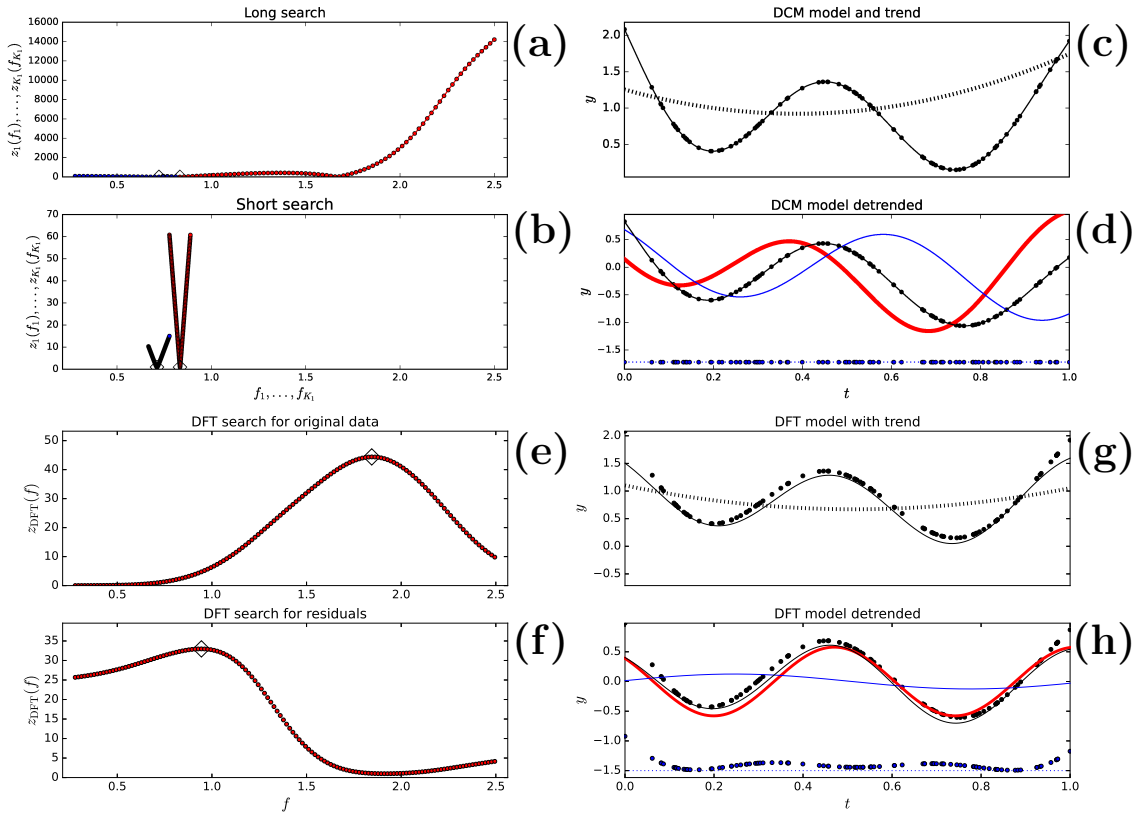


Fig. 7 Model 7 (Table 7: $n = 100$, SN = 5 000 000 simulation). Notations as in Figure 3. Best periods (diamonds) are explained in Section 3.7.

and $K_3 = 0$. We perform the DCM and DFT time series analysis between $P_{\min} = P_1/3 = 0.053$ and $P_{\max} = 3P_1 = 0.480$.

The DCM time series analysis results for different n and SN combinations are given in Table 6 (Columns 2-4). The DCM detects the correct P_1 , A_1 , $t_{1,\min,1}$, $t_{1,\min,2}$, $t_{1,\max,1}$, $t_{1,\max,2}$ and M_0 values even for the lowest $n = 50$ and SN = 10 combination. We demonstrate the DCM analysis results for simulated data having $n = 50$ and SN = 50 (Figures 6a-d). The long and short searches give $P_1 = 0.159$ (Figure 6a: diamond) and $P_1 = 0.160$ (Figure 6b: diamond). The DCM model $g(t)$ black line covers the black dots denoting the data y_i (Figure 6c). The "trend" at $p(t) = M_0 = -0.0055 \pm 0.0026$ is correct. The detrended model $g(t) - p(t)$ (black continuous line), the pure sine signal $h_1(t)$ (red thick continuous line) and the detrended data $y(t_i) - p(t_i)$ (black dots) are displayed in Figure 6d. The thick continuous red

line stays under the thin continuous black line because $h_1(t) = g(t) - p(t)$. The DCM residuals (blue dots) are offset to the level of -1.8 (blue dotted line). These residuals show no trends and their level is stable.

The DFT detects the wrong period $P_1 = 0.080$ (Figure 6e: Diamond). This results is exactly half of the correct simulated value $P_1 = 0.160$. The reason for this "detection" is that the double wave dominates because $c_2 = 2c_1$ in Model 6 (Equation 37). The DFT mean level estimate $M_0 = -0.172$ fails (Figure 6f: Dashed black line). The DFT analysis of the residuals $\epsilon_i = y(t_i) - [s_{y,\text{DFT}}(t_i) + p_{\text{DFT}}(t_i)]$ gives $P_2 = 0.161$, which is nearly equal to the correct simulated $P_1 = 0.160$ value. The black dots denoting the data y_i show minor deviations from continuous black line denoting the DFT model $g_{\text{DFT}}(t)$ (Figure 6g). The detrended model $g_{\text{DFT}}(t) - p_{\text{DFT}}(t)$ (continuous black line), the detrended data $y(t_i) - p_{\text{DFT}}(t_i)$ (black dots)

and the signal $s_{y,\text{DFT}}(t)$ (continuous thick red line) are shown in Figure 6h. The DFT analysis residuals (blue dots) are offset to the level of -1.5 (blue dotted line). These residuals display trends.

We conclude that the DFT “detects” the $P_1/2$ and P_1 periods, where P_1 is the correct simulated period value. However, the DFT two signal model is not the correct model for these Model 6 simulated data, which contain only one signal. If the correct period is P and the correct model is a double wave ($K_2 = 2$), the DCM pure sine model ($K_1 = 1$) analysis can also give the values $P/2$ and P .

The DCM analysis succeeds for Model 6 simulated data. The DFT analysis fails.

3.7 Model 7

In this section, we analyse our most complex data set. The seventh simulation model is

$$g(t) = c_1 \cos \left[\frac{2\pi t}{P_1} \right] + c_2 \cos \left[\frac{4\pi(t - c_3)}{P_1} \right] + c_4 \cos \left[\frac{2\pi t}{P_2} \right] + c_5 \cos \left[\frac{4\pi(t - c_6)}{P_2} \right] + M_0 + M_1 T + M_2 T^2 \quad (37)$$

where $T = [2(t - t_{\text{mid}})]/\Delta T$, $P_1 = 1.2$, $P_2 = 1.4$, $M_0 = 1$, $M_1 = 0.25$ and $M_2 = 0.5$. The coefficients $c_1 = 0.3687$, $c_2 = 0.7374$, $c_3 = 0.4000$, $c_4 = 0.3708$, $c_5 = 0.7416$ and $c_6 = 0.6000$ determine the A_1 , $t_{1,\text{min},1}$, $t_{1,\text{min},2}$, $t_{1,\text{max},1}$, $t_{1,\text{max},2}$, A_2 , $t_{2,\text{min},1}$, $t_{2,\text{min},2}$, $t_{2,\text{max},1}$ and $t_{2,\text{max},2}$ values given in Table 7 (Column 1). This simulated data sample is “too short” because $\Delta T < P_1 < P_2$ (Equation 27). The parabolic $p(t)$ represents “a trend” (Equation 28). The signal frequencies f_1 and f_2 are “too close” because $\Delta f = f_1 - f_2 = 0.12 < f_0 = 1$ (Equation 29). The two $h_1(t)$ and $h_2(t)$ signals are not “pure sines” (Equation 30). These signals are double waves having two unequal minima and maxima. All four main reasons that can cause the failure of DFT analysis are present (Equations 27-30). Therefore, this simulated data set is the most complex one of all analysed seven data sets. Our DCM and DFT time series analysis of Model 7 simulated data is performed between $P_{\text{min}} = P_1/3 = 0.4$ and $P_{\text{max}} = 3P_1 = 3.6$.

The DCM orders of Model 7 are $K_1 = 2$, $K_2 = 2$ and $K_3 = 2$. This model has $\eta = 13$ free

parameters (Equation 8). We give the DCM analysis results for different n and SN combinations in Table 7 (Columns 2-4). The DCM analysis results are displayed for one sample of Model 7 simulated data (Figures 7a-d: $n = 100$ and SN = 5 000 000). Since there are $\eta = 13$ free model parameters, this $n = 100$ sample is quite small for time series analysis. The long and short DCM searches give $P_1 = 1.200$ and $P_2 = 1.385$ (Figure 7a: diamonds), and $P_1 = 1.199$ and $P_2 = 1.405$ (Figure 7b: Diamonds). The black $g(t)$ model line goes through all black y_i data dots (Figure 7c). The DCM detects the correct polynomial trend $p(t)$ coefficients $M_0 = 0.950 \pm 0.050$, $M_1 = 0.2447 \pm 0.0067$ and $M_2 = 0.551 \pm 0.050$ (Figure 7c: dashed black line). The detrended DCM model $g(t) - p(t)$ (white continuous line), the detrended data $y(t_i) - p(t_i)$ (black dots), the signal $h_1(t)$ (red thick continuous line) and the signal $h_2(t)$ (blue thin continuous line) are displayed in Figure 7d. The $n = 100$ residuals (blue dots) are offset to the level of -1.8 (dotted blue line). These DCM model residuals are small and their level is stable. These results confirm that the DCM time series analysis method can detect complex non-linear models ($\eta = 13$) from very small data sets ($n = 100$), if these data are extremely accurate (SN = 5 000 000).

The DFT time series analysis gives the wrong periods for the original data (Figure 7e: diamond at $P_1 = 0.542$ and for the residuals (Figure 7f: diamond at $P_2 = 1.059$). The DFT also gives wrong $p(t)$ trend coefficients $M_0 = 0.670$, $M_1 = -0.025$ and $M_2 = 0.406$ (Figure 7g: dashed black line). The DFT model $g_{\text{DFT}}(t)$ (black continuous line) deviates from the data y_i (black dots). This deviation is largest at the beginning and the end of the simulated data sample. In our Figure 7h, the black dots denote the detrended data $y(t_i) - p_{\text{DFT}}(t_i)$, the continuous black line denotes the detrended DFT model $g_{\text{DFT}}(t) - p_{\text{DFT}}(t)$ and the continuous thick red line denotes pure sine signal $s_{y,\text{DFT}}(t)$ detected from the original data. The DFT model $g_{\text{DFT}}(t)$ gives very low amplitude for the pure sine signal $s_{\epsilon,\text{DFT}}(t)$ detected from the residuals (continuous thinner blue line). The correct simulated peak to peak amplitude for this second signal is much larger, $A_2 = 2$. The DFT model residuals (blue dots) are offset to -1.5 level and show strong trends.

The DCM time series analysis succeeds for Model 7 simulated data. The DFT time series analysis fails, as predicted by Equations 27-30.

3.8 Best model

The K_1 , K_2 and K_3 orders of the best model are not necessarily known when some time series analysis method is applied to the real data. We know a priori the best DCM and DFT model orders for the simulated data of Models 1-7 (Sections 3.1-3.7). It could be argued that our DCM analysis succeeds only for this reason.

All alternative K_1 , K_2 and K_3 order models are nested. For example, the *simple* one signal $K_1 = 1$ model $g_1(t)$ is a special case of the *complex* two signal $K_1 = 2$ model $g_2(t)$ having $A_2 = 0$. We use the Fisher-test to compare any pair of simple $g_1(t)$ and complex $g_2(t)$ models. The model parameters (Equation 13: R_1, R_2), (Equation 14: χ_1, χ_2) and (Equation 8: $\eta_1 < \eta_2$) give the test statistic of Fisher-test

$$F_R = \left(\frac{R_1}{R_2} - 1 \right) \left(\frac{n - \eta_2 - 1}{\eta_2 - \eta_1} \right) \quad (38)$$

$$F_\chi = \left(\frac{\chi_1^2}{\chi_2^2} - 1 \right) \left(\frac{n - \eta_2 - 1}{\eta_2 - \eta_1} \right). \quad (39)$$

The Fisher-test is based on the null hypothesis

H_0 : “The complex model $g_2(t)$ does not provide a significantly better fit to the data than the simple model $g_1(t)$.”

Under this hypothesis, the F_R and F_χ test statistic parameters have an F distribution with $\nu_1 = \eta_2 - \eta_1$ and $\nu_2 = n - \eta_2$ degrees of freedom (Draper and Smith 1998). The critical level $Q_F = P(F_R \geq F)$ or $Q_F = P(F_\chi \geq F)$ is the probability that F_R or F_χ exceeds the numerical value F . If

$$Q_F < \gamma_F = 0.001, \quad (40)$$

we reject the H_0 hypothesis, which means that the complex $g_2(t)$ model is better than the simple $g_1(t)$ model. The pre-assigned significance level $\gamma_F = 0.001$ represents the probability that we falsely reject the H_0 hypothesis when it is in fact true.

Larger F_R or F_χ values have smaller Q_F critical levels. Hence, the probability for the H_0 hypothesis rejection increases when F_R or F_χ

increases. If the number of complex model free parameters η_2 increases, the R_2 or χ_2^2 values decrease. This increases the F_R or F_χ values because the terms $(R_1/R_2 - 1)$ or $(\chi_1^2/\chi_2^2 - 1)$ increase (Equations 38 and 39: first terms). At the same time, the $(n - \eta_2 - 1)/(\eta_2 - \eta_1)$ penalty term decreases (Equations 38 and 39: second terms), and this decreases the F_R or F_χ values. This penalty term prevents the use of too high η_2 values (too complex models).

Here, we illustrate how the Fisher-test finds the best model from a group of numerous alternative nested DCM models. The Fisher-test is used to find the best model for the simulated data of Model 1 combination $n = 100$ and $\text{SN} = 100$ (Table 1: column 4). In other words, we assume that the correct DCM model orders K_1 , K_2 and K_3 are unknown, which can be the case for real data. The eight tested models contain one or two signals, and no trend or a constant trend or a linear trend or a parabolic trend. We compare all these eight models $\mathcal{M}=1-8$ against each other (Table 8). The special model number notation “ \mathcal{M} ” is used because the notations “ M_0, \dots, M_{K_3} ” have already been reserved for the $p(t)$ trend.

Model $\mathcal{M}=2$ has the known correct Model 1 orders $K_1 = 1$, $K_2 = 1$ and $K_3 = 0$. For example, the Fisher-test between the simple model $\mathcal{M}=1$ ($\eta = 3$, $\chi^2 = 738$) and the complex model $\mathcal{M}=2$ ($\eta = 4$, $\chi^2 = 84.7422$) gives $F = 733$ (Equation 39). The critical level³ for this very large F value is extremely significant, $Q_F < 10^{-16}$. This means that the H_0 hypothesis must be rejected, and the complex $\mathcal{M}=2$ model is certainly better than the simple $\mathcal{M}=1$ model (Equation 40). The upward arrow “ \uparrow ” in Table 8 indicates that $\mathcal{M}=2$ model is a better model than $\mathcal{M}=1$ model. A closer look at Table 8 reveals that $\mathcal{M}=2$ model is better than all other models because the “ \uparrow ” and “ \leftarrow ” arrows of all other models point toward $\mathcal{M}=2$ model. There is no need to test models having more than two signals because all two signal $\mathcal{M}=5-8$ models are already unstable (Table 8: “UM”). The Fisher-test finds the correct DCM model for Model 1 simulated data.

³The highest achievable accuracy for the computational f.cdf subroutine in scipy.optimize python library is 10^{-16} .

Table 8 Fisher tests: DCM analysis of Model 1 simulated data ($n = 100$, SN = 100, data file Model1In100SN100). (1) Simple model: Model number \mathcal{M} , model g_{k_1, k_2} , number of free parameters η , chi-square χ^2 and control file name. (2-8) Complex model: Hypothesis H_0 rejected \uparrow (Complex model better), Hypothesis H_0 not rejected \leftarrow (Simple model better), test statistic F and critical level Q_F .

(1)	(2)	(3)	(4)	(5)	(6)	(7)	(8)
Simple model	Complex model						
	$\mathcal{M}=2$	$\mathcal{M}=3$	$\mathcal{M}=4$	$\mathcal{M}=5$	$\mathcal{M}=6$	$\mathcal{M}=7$	$\mathcal{M}=8$
$\mathcal{M}=1$	\uparrow	\uparrow	\uparrow	\uparrow	\uparrow	\uparrow	\uparrow
$g_{1,,1,-1}$	$F = 733$	$F = 367$	$F = 242$	$F = 242$	$F = 180$	$F = 142$	$F = 121$
$\eta = 3, \chi^2 = 738$	$Q_F < 10^{-16}$	$Q_F < 10^{-16}$	$Q_F < 10^{-16}$	$Q_F < 10^{-16}$	$Q_F < 10^{-16}$	$Q_F < 10^{-16}$	$Q_F < 10^{-16}$
dcmModel11K11-1.dat							
$\mathcal{M}=2$	-	\leftarrow	\leftarrow	\leftarrow	\leftarrow	\leftarrow	\leftarrow
$g_{1,1,0}$	-	$F = 1.0451$	$F = 0.5404$	$F = 0.5159$	$F = 0.3553$	$F = 0.2784$	$F = 0.7686$
$\eta = 4, \chi^2 = 84.7422$	-	$Q_F = 0.309$	$Q_F = 0.584$	$Q_F = 0.599$	$Q_F = 0.785$	$Q_F = 0.891$	$Q_F = 0.575$
dcmModel11K110.dat							
$\mathcal{M}=3$	-	-	\leftarrow	\leftarrow	\leftarrow	\leftarrow	\leftarrow
$g_{1,1,1}$	-	-	$F = 0.0464$	$F = -0.0021$	$F = 0.0213$	$F = 0.0336$	$F = 0.7027$
$\eta = 5, \chi^2 = 83.8104$	-	-	$Q_F = 0.830$	$Q_F = 1$	$Q_F = 0.979$	$Q_F = 0.992$	$Q_F = 0.592$
dcmModel11K111.dat							
$\mathcal{M}=4$	-	-	-	\leftarrow	\leftarrow	\leftarrow	\leftarrow
$g_{1,1,2}$	-	-	-	No test ¹	$F = -0.0033$	$F = 0.0277$	$F = 0.9215$
$\eta = 6, \chi^2 = 83.7686$	-	-	-		$Q_F = 1$	$Q_F = 0.973$	$Q_F = 0.434$
dcmModel11K112.dat							
$\mathcal{M}=5$ UM : AD	-	-	-	-	\leftarrow	\leftarrow	\leftarrow
$g_{2,1,-1}$	-	-	-	-	$F = 0.0447$	$F = 0.0515$	$F = 0.9377$
$\eta = 6, \chi^2 = 83.8123$	-	-	-	-	$Q_F = 0.833$	$Q_F = 0.950$	$Q_F = 0.426$
dcmModel11K21-1.dat							
$\mathcal{M}=6$ UM : IF, AD	-	-	-	-	-	\leftarrow	\leftarrow
$g_{2,1,0}$	-	-	-	-	-	$F = 0.0587$	$F = 1.3840$
$\eta = 7, \chi^2 = 83.7716$	-	-	-	-	-	$Q_F = 0.809$	$Q_F = 0.256$
dcmModel11K210.dat							
$\mathcal{M}=7$ UM : IF, AD	-	-	-	-	-	-	\leftarrow
$g_{2,1,1}$	-	-	-	-	-	-	$F = 2.7081$
$\eta = 8, \chi^2 = 83.7176$	-	-	-	-	-	-	$Q_F = 0.103$
dcmModel11K211.dat							
$\mathcal{M}=8$ UM : IF, AD	-	-	-	-	-	-	-
$g_{2,1,2}$	-	-	-	-	-	-	-
$\eta = 9, \chi^2 = 81.2721$	-	-	-	-	-	-	-
dcmModel11K212.dat							

Table 9 Fisher tests for Model 1
 $n = 100$, $\text{SN} = 100$ simulated data (electronic data file `Model1n100SN100`). (1) Polynomial model. (2) DCM model $g_{1,1,0}$. Note that $\mathcal{M}=1-3$ polynomials represent simple models, and $\mathcal{M}=5-8$ polynomials represent complex models. Otherwise as in Table 8.

(1)	(2)
Polynomial	$\eta = 4, \overset{g_{1,1,0}}{\chi^2} = 84.7422$
$\mathcal{M}=1$	↑
$g(t) = p(t, K_3 = 0)$	$F = 63218$
$\eta = 1, \chi^2 = 169260$	$Q_F < 10^{-16}$
$\mathcal{M}=2$	↑
$g(t) = p(t, K_3 = 1)$	$F = 54366$
$\eta = 2, \chi^2 = 97076$	$Q_F < 10^{-16}$
$\mathcal{M}=3$	↑
$g(t) = p(t, K_3 = 2)$	$F = 1945$
$\eta = 3, \chi^2 = 1820$	$Q_F < 10^{-16}$
$\mathcal{M}=4$	↑
$g(t) = p(t, K_3 = 3)$	No test ¹
$\eta = 4, \chi^2 = 469$	
$\mathcal{M}=5$	↑
$g(t) = p(t, K_3 = 4)$	$F = -0.3718$
$\eta = 5, \chi^2 = 85.0787$	$Q_F = 1$
$\mathcal{M}=6$	↑
$g(t) = p(t, K_3 = 5)$	$F = 0.3403$
$\eta = 6, \chi^2 = 84.1265$	$Q_F = 0.712$
$\mathcal{M}=7$	↑
$g(t) = p(t, K_3 = 6)$	$F = 0.3524$
$\eta = 7, \chi^2 = 83.7794$	$Q_F = 0.787$
$\mathcal{M}=8$	↑
$g(t) = p(t, K_3 = 7)$	$F = 0.9394$
$\eta = 8, \chi^2 = 81.3819$	$Q_F = 0.445$

Note: No Fisher-test for $\mathcal{M}=4$ ($\eta_1 = \eta_2 = 4$).

In the above example, the Fisher-test finds the correct number of signals (K_1) and the correct trend (K_3) for the pure sine signal alternative ($K_2 = 1$). We do not test the double wave signal alternative ($K_2 = 2$) against the pure sine signal alternative ($K_1 = 1$) because the number of tested models would increase from 8 to 16, and Table 8 would become excessively large. One example of testing the $K_2 = 2$ signal models against each other can be found in Jetsu (2025, Table S7).

We conclude that the best model for the real data can be found by applying the Fisher-test to any arbitrary number of different nested DCM or DFT models.

3.9 Significance estimates

The Fisher-test gives the critical level Q_F for rejecting the H_0 hypothesis (Equation 40). After the detection of the first strongest signal, the values Q_F of these critical levels increase for the next detected weaker signals. Typical examples can be found in Jetsu 2025 (Tables S5-S16). No new signals are detected when $Q_F > \gamma = 0.001$ because the critical level exceeds the pre-assigned significance level and the H_0 hypothesis is no longer rejected.

The Fisher test critical level Q_F is the significance estimate for each signal detected after the first signal. However, this Fisher-test process gives no significance estimate for the first detected signal.

We estimate the critical level Q_F for the first detected signal $h_1(t)$ by testing the alternative that there are no signals in the data. The “no signal hypothesis” is

$$h(t) = 0 \Rightarrow h_1(t) = 0 \Rightarrow g(t) = p(t). \quad (41)$$

In Model 1 simulated data combination $n = 100$ and $\text{SN} = 100$, the correct model is $g_{1,1,0}(t)$. We use the Fisher-test to compare this correct $g_{1,1,0}(t)$ model to different polynomial models $g(t) = p(t)$ having $K_3 = 0, 1, \dots, 7$ (Table 9).

The $\mathcal{M}=1, 2$ and 3 models have less free parameters than the correct $g_{1,1,0}(t)$ model, but the χ^2 values of these three polynomial models are so large that the Fisher-test is merely a formality. The $\mathcal{M}=4$ model has the same number of free parameters as the correct $g_{1,1,0}(t)$ model, but the comparison of χ^2 values reveals that this third order $p(t)$ polynomial is not the correct model for the data. The next model $\mathcal{M}=5$ has more free parameters than the correct $g_{1,1,0}(t)$ model. This fourth order $p(t)$ polynomial $\mathcal{M}=5$ model must be rejected because it has a larger χ^2 value than the correct $g_{1,1,0}(t)$ model. The critical levels $Q_F \gg \gamma = 0.001$ for the remaining $\mathcal{M}=6, 7$ and 8 polynomial models are so large that these models must also be rejected. The results in Table 9 confirm the “no signal hypothesis” (Equation 41) rejection. The analysed Model 1 simulated data must contain at least the $h_1(t)$ pure sine signal. For the constant, linear or parabolic $p(t)$ trend alternatives, the critical level for this $h_1(t)$ signal is $Q_F < 10^{-16}$.

There is no need to discuss the DFT significance estimates (Horne and Baliunas 1986, their Equation 22) because this method fails to detect the correct Model 1 period.

3.10 Prediction

There are numerous techniques for predicting (forecasting) a time series (e.g., Hamilton 1994; Hastie et al. 2001; Kazemi and Rodrigues 2025). The DCM model $g(t_i, \beta)$ can be used to predict. We divide all data into the predictive data and the predicted data. The time points, the observations and the errors of these samples are

n predictive data values t_i, y_i and σ_i
 n' predicted data values t'_i, y'_i and σ'_i

The DCM gives the best predictive data model

$$g_i = g(t_i, \beta_{\text{pred}}), \quad (42)$$

where β_{pred} are the free parameter values. The $t_{\text{mid,pred}} = (t_n + t_1)/2$ and $\Delta T_{\text{pred}} = t_n - t_1$ values are computed from the predictive data time points t_i .

The predicted data model values are

$$g'_i = g(t'_i, \beta_{\text{pred}}), \quad (43)$$

where $t_{\text{mid}} = t_{\text{mid,pred}}$ and $\Delta T = \Delta T_{\text{pred}}$. We do not compute “new” t_{mid} and ΔT values from the predicted data time points t'_i because the correct g'_i values are obtained only from the β_{pred} , $t_{\text{mid,pred}}$ and ΔT_{pred} combination of Equation 42. The n' predicted data model residuals

$$\epsilon'_i = y'_i - g'_i$$

give the *predicted data test statistic*

$$z_{\text{pred}} = z \text{ test statistic for predicted data } t'_i, y'_i \text{ and } \sigma'_i \text{ (Equation 15 or 16)}. \quad (44)$$

This parameter z_{pred} measures how well the prediction (Equation 43) obtained from the predictive data works for the predicted data. If the DCM detects a new signal from the predictive data, there are two alternatives:

If this new signal is real, the z_{pred} value of predicted data decreases.

If this new signal is unreal, the z_{pred} value of predicted data increases.

This “Prediction-test” technique revealed at least five real signals in the sunspot record (Jetsu 2025).

We compute the z_{pred} parameter value from the *known* predicted data t'_i, y'_i and σ'_i values (Equation 44). Predictions are possible even if all t'_i, y'_i or σ'_i predicted data values are *unknown*. In this case, the t_i, y_i and σ_i values of all data can be used as predictive data. The best DCM model $g(t_i, \beta_{\text{pred}})$ for all data determines the correct β_{pred} , $t_{\text{mid,pred}} = (t_n + t_1)/2$ and $\Delta T_{\text{pred}} = t_n - t_1$ combination. The n' predicted data time points t'_i can be created for any arbitrary chosen time interval $\Delta T' = t'_n - t'_1$. The n' predicted model $g'_i = g'_i(t'_i, \beta_{\text{pred}})$ values are obtained from Equation 43. These g'_i values can be used, for example, to compute the *predicted mean level*

$$m_{\text{pred}} = \frac{1}{n'} \sum_{i=1}^{n'} g'_i \quad (45)$$

during the chosen time interval $\Delta T' = t'_n - t'_1$. Jetsu (2025) used this m_{pred} parameter to postdict the known $\Delta T'$ time intervals of prolonged solar activity minima, like the Maunder minimum between the years 1640 and 1720. Since the known mean level of all sunspot data was m , Jetsu (2025) used these three criteria for correct postdictions of past prolonged activity minima $\Delta T'$ time intervals:

If DCM detects a real new signal in all data, the m_{pred} value decreases.

If DCM detects many real signals in all data, the m_{pred} value falls below m .

If DCM detects an unreal new signal in all data, the m_{pred} value increases.

We use Model 3 combination $n = 50$ and $\text{SN} = 10$ simulated data (Table 3, column 2) to illustrate the DCM prediction technique. The black dots in Figures 8a-c are the first $n = 40$ predictive data values t_i, y_i and σ_i . The open black dots denote the $n' = 10$ predicted data values t'_i, y'_i and σ'_i . The continuous black line is the predictive model $g(t)$ and the dotted black line is the predicted model $g'(t)$. The red dotted line shows the $\pm 3\sigma$ errors of both models. The blue dots are the predictive data $\epsilon_i = y_i - g_i$ residuals and the open blue dots are the predicted data $\epsilon'_i = y'_i - g'_i$ residuals.

Model 3 is the sum of two $P_1 = 0.16$ and $P_2 = 0.17$ pure sine signals ($K_1 = 2, K_2 = 1$)

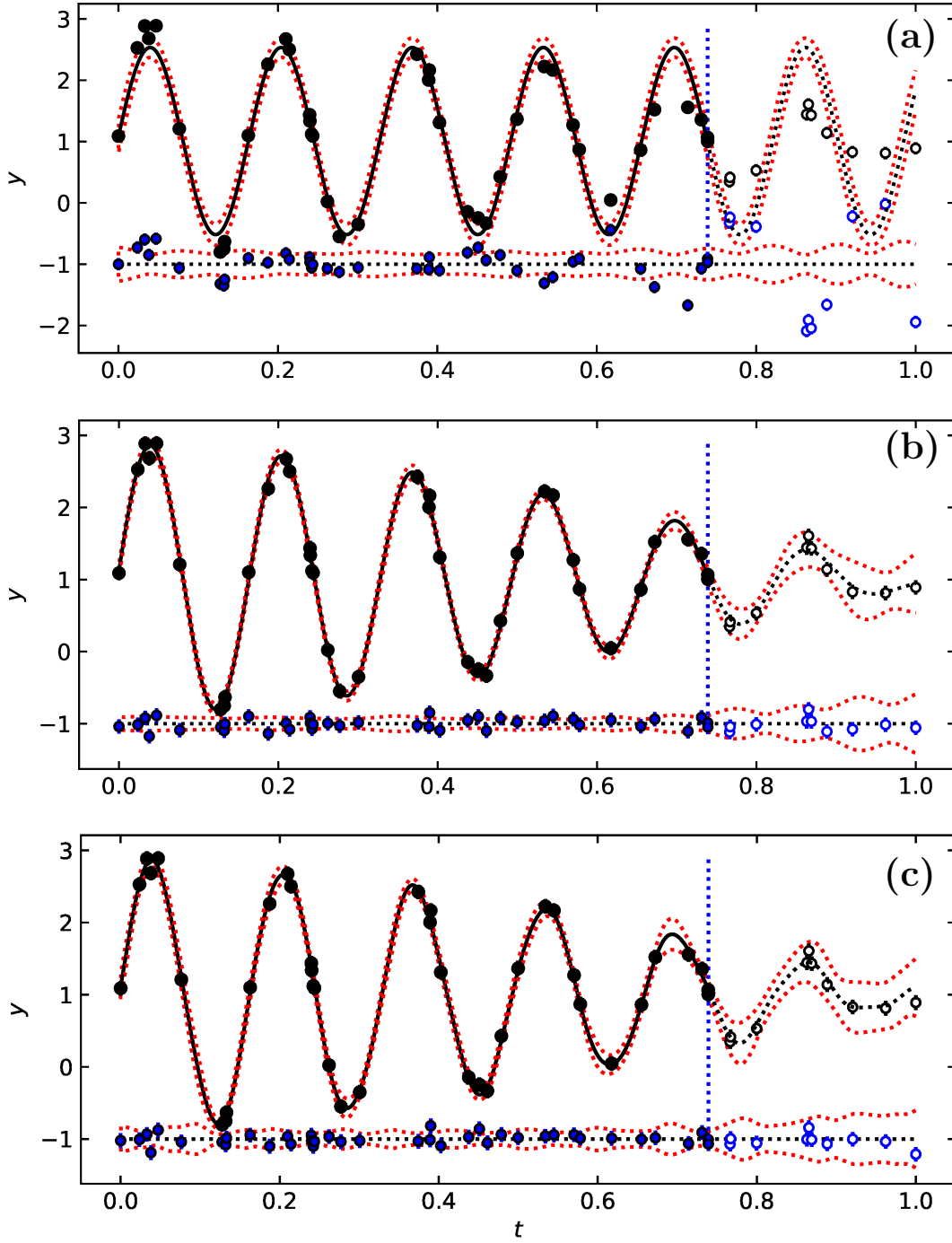


Fig. 8 DCM model prediction (Model 3 simulated data for combination $n = 50$ and $\text{SN} = 10$: first forty observations are predictive data). (a) One signal model $g_{1,1,0}$ results. Predictive data are t_i, y_i and σ_i ($n = 40$ black dots) and predicted data are ten last observations t'_i, y'_i and σ'_i ($n = 10$ open black dots). Continuous black line of predictive data model $g(t, \beta_{\text{pred}})$ ends to vertical dotted blue line, where dotted black line of predicted model $g'(t, \beta_{\text{pred}})$ begins. Dotted red line denotes $\pm 3\sigma_{g(t)}$ errors of both models (Equation 22). Residuals of predictive data model $\epsilon_i = y_i - g_i$ (blue dots), residuals of predicted data model $\epsilon'_i = y'_i - g'_i$ (open blue dots) and $\pm 3\sigma$ errors of both models (red dotted line) are offset to level -1 (blue dotted line). (b) Two signal model $g_{2,1,0}$ results. Otherwise as in “a”. (c) Three signal model $g_{3,1,0}$ results. Otherwise as in “a”.

Table 10 DCM time series analysis between $P_{\min} = 0.53$ and $P_{\max} = 4.80$ for predictive data (Model = 3 combination $n = 50$ and SN = 10 simulated data: first forty observations). (1) Model. (2) Predictive data test statistic z (Equation 16). (3) Predicted data test statistic z_{pred} (Equation 44). (4) Data file. (5) Control file. (6) Figure where prediction is shown.

(1) Model	(2) z	(3) z_{pred}	(4) Data file	(5) Control file	(6) Figure
$g_{1,1,0}$	2.27	8.61	Model13n40SN10.dat	dcmModel13K110.dat	8a
$g_{2,1,0}$	0.76	0.88	Model13n40SN10.dat	dcmModel13K210.dat	8b
$g_{3,1,0}$	0.70	0.91	Model13n40SN10.dat	dcmModel13K310.dat	8c

superimposed on the constant mean level $M_0 = 1$ ($K_3 = 0$). We compute the z and z_{pred} values for the $g_{1,1,0}$, $g_{2,1,0}$ and $g_{3,1,0}$ models (Table 10). These three models have the same $K_2 = 1$ and $K_3 = 0$ orders as Model 3, but their signal numbers $K_1 = 1, 2$ or 3 are different, the $g_{2,1,0}$ model being the correct simulation Model 3.

The correct $g_{2,1,0}$ model gives the smallest $z_{\text{pred}} = 0.88$ value (Table 10). Therefore, it is a better predictive model than the $g_{1,1,0}$ and $g_{3,1,0}$ models. The one signal $g_{1,1,0}$ model prediction fails because the blue open circles denoting the predicted data residuals $\epsilon'_i = y'_i - g'_i$ show large deviations from the blue dotted line offset level of $\epsilon'_i = -1$ (Figure 8a). The two signal $g_{2,1,0}$ model prediction succeeds because all open blue dots denoting the predicted data residuals stay close to the blue dotted line offset level $\epsilon'_i = -1$, as well as inside the red dotted $\pm 3\sigma$ model error limits (Figure 8b).

The three signal model $g_{3,1,0}$ periods are $P_1 = 0.0643 \pm 0.0018$, $P_2 = 0.1592 \pm 0.0012$ and $P_3 = 0.1716 \pm 0.0012$. The amplitudes of these pure sine signals are $A_1 = 0.092 \pm 0.025$, $A_2 = 1.879 \pm 0.16$ and $A_3 = 1.82 \pm 0.15$. The periods and the amplitudes of the two strongest P_2 and P_3 signals are correct because they are the same as in Model 3 simulation (Table 3, column 1). Therefore, the $g_{3,1,0}$ prediction appears nearly as good as the $g_{2,1,0}$ prediction because the residuals ϵ'_i are close to the offset level of $\epsilon'_i = -1$ (blue open dots), and these residuals also stay inside the red dotted $\pm 3\sigma$ model error limits (Figure 8c). The amplitude $A_1 = 0.092$ of the third $P_1 = 0.0643$ signal is very low. Due this weak “unreal” P_1 signal, the $g_{3,1,0}$ model has a larger $z_{\text{pred}} = 0.91$ value than the correct $g_{2,1,0}$ model (Table 10).

The $n = 40$ predictive data parameters $\eta_1 = 7$, $\eta_2 = 10$, $\chi_1 = 22.946$ and $\chi_2 = 19.790$ for the simple $g_{2,1,0}$ model and the complex $g_{3,1,0}$ model give

Fisher-test values $F_\chi = 1.32$ and $Q_F = 0.28 > \gamma_F = 0.001$. The H_0 hypothesis is not rejected. For the predictive data, the Fisher-test also confirms that the $g_{2,1,0}$ model is better than the $g_{3,1,0}$ model. Finally, we note that the three signal model $g_{3,1,0}$ is not unstable (“UM”) although the simulated data contains only two signals.

For the $g_{2,1,0}$ model, the DCM detects the correct Model 3 signal frequencies (Table 3), but these frequencies are “too close” for the correct DFT detection (Equation 29). Therefore, the DFT prediction can not succeed.

The analyses of all seven complex data sets indicate that the relative accuracy of amplitude and period estimates are lower than the relative accuracy of signal minimum and maximum epoch estimates (Tables 1 - 7). This statistical effect is the same when DCM is applied to the data of any arbitrary phenomenon. This effect would, for example, explain why our solar cycle amplitude predictions are less accurate than our solar cycle minimum and maximum epoch predictions (Jetsu 2025). DCM detects the correct simulated period values, but DFT detects less accurate period values, which are not always correct. The leakage of DFT spectral power (Kay and Marple 1981; Ghaderpour et al. 2021) would explain why correct signal periods have not been detected earlier from the sunspot data.

4 Discussion

The solution for the non-linear DCM model is an ill-posed problem (Equations 1-5). We present a computational statistical solution that fulfils the C_1 , C_2 and C_3 conditions of a well-posed problem. The DCM model is just one special case of a non-linear model. Our technique can be applied to solve other non-linear models: Use the free parameters that make the model non-linear

(Equation 9: β_I) for solving the remaining other free parameters (Equation 10: β_{II}).

4.1 Existence (C_1)

Fourier (1822) transformed the original function into the frequency domain. The modern DFT time series analysis method transforms the original data into the frequency domain and gives the best frequency for a pure sine model. Gauß (1821) presented the least squares method, which minimises the differences between the data and the linear model. Our DCM does the same by testing a large number of linear models. The data spacing, even or uneven, is irrelevant for these models. For every chosen DCM model, the number of tested linear models is

$$\binom{n_L}{K_1} + (1 + n_B) \times \binom{n_S}{K_1}, \quad (46)$$

where the number of tested long and short search frequencies is n_L and n_S , respectively. The number of bootstrap samples is n_B . In other words, we solve this ill-posed problem by using brute computational force. If the data contain only zero mean white noise, the Gauß-Markov theorem ensures that a linear least squares fit solution *exists* for every tested frequency combination.

4.2 Uniqueness (C_2)

We make the most of the Gauß-Markov theorem. When the numerical values of the tested frequencies β_I (Equation 9) are fixed, the model becomes linear and the solution for the other free parameters β_{II} is *unique* (Equation 10). All possible β_I frequency combinations are tested (Equation 11). For every tested frequency combination β_I , the linear model gives a *unique* value for the test statistic z (Equations 15 and 16). From all tested frequency combinations, we select the best frequency combination $\beta_{I,\text{best}}$ which minimises z . The linear model for this best frequency combination $\beta_{I,\text{best}}$ gives *unique* values for the remaining other free parameters $\beta_{II,\text{best}}$. The only goal for the massive DCM search (Equation 46) is to find these *unique* initial free parameter values $\beta_{\text{initial}} = [\beta_{I,\text{best}}, \beta_{II,\text{best}}]$ for the non-linear iteration that gives the *unique* final free parameter values β_{final} (Equation 21).

We use the Fisher-test to compare many different non-linear DCM models against each other. The selection criterion for the best model is *unique* (Equation 40). The best DCM model is not necessarily the correct model, if this correct model is not among the compared models. The correct model must be able to predict the future and past data. We formulate the Predictability-test for alternative DCM models (Equation 44). The order of Fisher- and Predictability-tests can be reversed. However, the former uses all data, while the latter uses a subset of all data, the predictive data. In ideal cases, both tests identify the same best and correct model, like in Section 3.10.

4.3 Stability (C_3)

The artificial bootstrap data sets (Equation 23) represent “small changes in the input data”, while the bootstrap results for the model parameters represent “small changes in the solution” (Section 1: C_3 condition formulation). We routinely check the *stability* of these solutions (e.g. Jetsu 2025, Figure S5). The unstable models, where the model parameter changes are large, are rejected (Section 2.1: “UM” models).

There are additional signatures of *stability*. The z periodogram solution is unique for every tested β_I frequency combination. If these periodograms are continuous and their changes are not irregular (e.g., like in Figs. 1a-b), the DCM model solution is *stable* because it does not change by increasing the number of tested frequencies n_L and n_S . Furthermore, the solutions for all seven simulated data sets converge when the n and SN values increase (Tables 1 - 7). The different n and SN combinations give the same *stable* DCM model solution.

We conclude that our computational statistical DCM model solution fulfils the C_1 , C_2 and C_3 conditions of the solution for a well-posed problem (Sections 4.1 - 4.3).

4.4 Performance

DCM does not suffer from the DFT limitations (Equations 27-30). The simulated complex data sets of Models 1-7 expose these DFT weaknesses, but in all these cases, DCM detects all periodic signals superimposed on an unknown trend (Sections 3.1 - 3.7). The correct signal(-s) and trend are

detected. If there is enough (n) very accurate (σ_i) data (y_i), DCM can predict the future or postdict the past by finding the correct DCM model for these data. We do admit that the n and SN values of Models 2, 5 and 7 are extreme and unrealistic for most cases of real data. However, those model simulations are necessary for demonstrating that DCM can detect signals from short ΔT samples of high quality data. Those DCM signal detections depend only on the number of observations and their accuracy.

Our DCM computes the R (Equation 13) or χ^2 (Equation 14) values for a massive number of linear models (Equation 46). The Gauß-Markov theorem ensures that the model having the lowest R or χ^2 is eventually *always* found, and the result for the non-linear iteration is unique (Equation 21). We could have simulated more complex data sets by increasing the values of K_1 (number of signals), K_2 (signal shape) and K_3 (polynomial order of trend). DCM would eventually detect those signals and the trend when the sampled data sets get larger (n) and/or the signal to noise ratio becomes higher (SN). In this sense, DCM has no limit for the complexity of the data sets. In the real world, it may be impossible to eliminate noise (SN), but it is possible increase the sample size (n). Since the time span (ΔT) is irrelevant, the best solution is fast sampling of accurate data sets. For example, many observers could measure the same phenomenon simultaneously. We recommend such fast sampling combined to DCM parallel computation Python code analysis.

We want to draw attention to three aspects of DCM computational performance.

1. Practical time series analysis applications, like digital signal processing, require fast computational algorithms (Kay and Marple 1981). Our computational statistical solution for the non-linear DCM model requires a lot of CPU. Yet, the CPU used is beside the point if a well-posed computational solution can be found to any challenging scientific non-linear problem. DCM proceeds through two stages. For every chosen alternative model, DCM performs a massive number of linear least squares fits (Equation 18) to find the unique initial free parameter values for the non-linear iteration (Equation 21). This first stage devours CPU. The second

fast stage, the Fisher-test, then reveals the best model alternative (Equation 40).

2. Our frequency space symmetry idea dramatically reduces CPU (Equation 11). For example, were this symmetry not exploited, the four signal $K_1 = 4$ search would give $4! = 24$ exactly the same solutions from four-dimensional tested grid in frequency space. This would cause unnecessary use of CPU in the preliminary testing all possible frequency combinations inside a tesseract (a four-dimensional cube). After one necessary iteration of Equation 21, and 23 unnecessary ones, the identification of the best frequency combination would be a daunting exercise.
3. The DCM signal detections depend only on the sample size n and the signal to noise ratio SN, but not on the time span ΔT . This dimensional effect makes sense. If the t_i and y_i data are inside a rectangle $\Delta T \times \Delta y = (t_n - t_1) \times [\max(y_i) - \min(y_i)]$, then the y_i/σ_i ratio reveals or hides the g_i model details. Since the time span of data ΔT is irrelevant, DCM is an ideal forecasting method. We have been deluded into unnecessary waiting for the repetition of the signal(-s). DCM can perceive the future and the past much “earlier” (from shorter ΔT) than previously thought, like in Equations 27 and 29. This should motivate fast sampling of large high quality data sets and their analysis using the DCM parallel Python code. The invention of computers has made it possible to use this computational statistical method, which is probably the simplest possible one.

The *analytical* solution for the non-linear DCM model is ill-posed (Equation 1). Regardless of the data set complexity, DCM can find a well-posed *computational statistical* solution for this problem (Equation 21). So far, we have compared DCM only to DFT. Both methods are parametric and operate in the frequency-domain. There are innumerable similar parametric time series analysis methods (e.g. Kay and Marple 1981; Ghaderpour et al. 2021). Each one of these other time series analysis methods suffers from their own particular application limitations. We list some of those application limitations below.

1. The required data spacing is even or uneven.
2. The number of signals is unknown.
3. The presence and shape of trend are unknown.

4. The degree of noise is unknown.
5. The sample window causes leakage.
6. The leakage weakens frequency resolution.
7. The signal frequencies are too close.
8. The signal periods exceed the data time span.
9. The signal shapes are not pure sinusoids.
10. The forecasts of non-linear models fail.

DCM does not suffer from any of these application limitations. This simple computational statistical method can fail if, and only if, the Gauß-Markov theorem is not valid. That is impossible.

Acknowledgements. This work has made use of NASA’s Astrophysics Data System (ADS).

Author contribution. Lauri Jetsu created the simulated data sets, performed the DCM and DFT analysis and wrote the manuscript.

Consent for publication. The author of this manuscript grants permission for the publication in *Computational Statistics*.

Data availability. All data files and all DCM control files are stored to <https://zenodo.org/uploads/17018676>.

Code availability. The DCM and Fisher-test Python codes are stored to <https://zenodo.org/uploads/17018676>. There is also a manual of how to use those codes.

Declarations

Competing interests. Lauri Jetsu declares no competing interests.

Funding. Lauri Jetsu declares that no funding was received for the conduct of this research or the preparation of this manuscript.

Ethics approval and consent to participate. Not applicable.

References

Bard, Y.: *Nonlinear Parameter Estimation*. Academic Press, New York, NY (1974)

Brockwell, P.J., Davis, R.A.: *Time Series: Theory and Methods*. Springer, New York, NY (2009)

Berger, J.O.: *Statistical Decision Theory and Bayesian Analysis*. Springer, London (2013)

Bisaglia, L., Gerolimetto, M.: Model-based inar bootstrap for forecasting inar (p) models. *Computational Statistics* **34**(4), 1815–1848 (2019)

Box, G.E., Jenkins, G.M., Reinsel, G.C., Ljung, G.M.: *Time Series Analysis: Forecasting and Control*. John Wiley & Sons, Hoboken, New Jersey (2015)

Bretthorst, G.L.: Excerpts from bayesian spectrum analysis and parameter estimation. In: *Maximum-Entropy and Bayesian Methods in Science and Engineering: Foundations*, pp. 75–145. Springer, London (1988)

Cleveland, R.B., Cleveland, W.S., McRae, J.E., Terpenning, I.: Stl: A seasonal-trend decomposition procedure based on loess. *Journal of Official Statistics* **6**(1), 3–73 (1990)

Draper, N.R., Smith, H.: *Applied Regression Analysis*. John Wiley & Sons, Inc., Hoboken, New Jersey (1998). <https://doi.org/10.1002/9781118625590>

Engl, H.W., Hanke, M., Neubauer, A.: *Regularization of Inverse Problems. Mathematics and Its Applications*. Kluwer Academic Publishers Group, Dordrecht (1996)

Efron, B., Tibshirani, R.: *Bootstrap Methods for Standard Errors, Confidence Intervals, and Other Measures of Statistical Accuracy*. *Statistical Science* **1**, 54 (1986)

Furlan, C., Mortarino, C.: Comparison among simultaneous confidence regions for nonlinear diffusion models. *Computational Statistics* **35**(4), 1951–1991 (2020)

Fourier, J.B.J.: *Théorie Analytique de la Chaleur*, (1822)

Gauß, K.F.: *Theoria Motv Corporvm Coelestivm in Sectionibvs Conicis Solem Ambientivm.*, (1809)

Gauß, C.F.: *Theoria Combinationis Observationum Erroribus Minimis Obnoxiae. Commentationes Societatis Regiae Scientiarum Göttingensis Recentiores* **1**, 1–94 (1821)

- Ghaderpour, E., Pagiatakis, S.D., Hassan, Q.K.: A survey on change detection and time series analysis with applications. *Applied Sciences* **11**(13) (2021) <https://doi.org/10.3390/app11136141>
- Hadamard, J.: Sur les problèmes aux dérivées partielles et leur signification physique. *Princeton University Bulletin* **13**, 49–52 (1902)
- Hadamard, J.: Lectures on Cauchy’s Problem in Linear Partial Differential Equations. Mrs. Hepsa Ely Silliman memorial lectures. Yale University Press, New Haven, Connecticut (1923)
- Hamilton, J.D.: Time Series Analysis. Princeton University Press, Princeton (1994). <https://doi.org/10.1515/9780691218632>
- Horne, J.H., Baliunas, S.L.: A Prescription for Period Analysis of Unevenly Sampled Time Series. *Astrophys. J.* **302**, 757 (1986) <https://doi.org/10.1086/164037>
- Hastie, T., Tibshirani, R., Friedman, J.: The Elements of Statistical Learning. Springer Series in Statistics. Springer, New York, NY, USA (2001)
- Jetsu, L.: Discrete Chi-square Method for Detecting Many Signals. *The Open Journal of Astrophysics* **3**(1), 4 (2020) <https://doi.org/10.21105/astro.2002.03890> [arXiv:2002.03890](https://arxiv.org/abs/2002.03890)
- Kay, S.M., Marple, S.L.: Spectrum analysis—a modern perspective. *Proceedings of the IEEE* **69**(11), 1380–1419 (1981) <https://doi.org/10.1109/PROC.1981.12184>
- Kazemi, M., Rodrigues, P.C.: Robust singular spectrum analysis: comparison between classical and robust approaches for model fit and forecasting. *Computational Statistics* **40**(6) (2025)
- Legendre, A.-M.: Nouvelles méthodes pour la détermination des orbites des comètes. *Journal de l’École Polytechnique* (1805)
- Lavrentiev, M.M., Romanov, V.G., Shishatskii, S.P.: Ill-posed Problems of Mathematical Physics and Analysis. *Translations of Mathematical Monographs*, vol. 64. American Mathematical Society, Providence, R.I. (1986)
- Nerlove, M.: Spectral analysis of seasonal adjustment procedures. *Econometrica: Journal of the Econometric Society*, 241–286 (1964)
- Rudin, W.: Principles of Mathematical Analysis. International series in pure and applied mathematics. McGraw-Hill, New York, NY (1976)
- Shumway, R.H., Stoffer, D.S.: Time Series Analysis and Its Applications: with R Examples. Springer, New York, NY (2006)
- Su, E.C.-Y., Wu, H.-M.: Dimension reduction and visualization of multiple time series data: a symbolic data analysis approach. *Computational Statistics* **39**(4), 1937–1969 (2024)
- Tikhonov, A.N., Arsenin, V.Y.: Solutions of Ill-posed Problems, p. 258. V. H. Winston & Sons, Washington, D.C.: John Wiley & Sons, New York (1977). Translated from the Russian, Preface by translation editor Fritz John, Scripta Series in Mathematics
- Tsay, R.S., Chen, R.: Nonlinear Time Series Analysis. Wiley Series in Probability and Statistics. John Wiley & Sons, Hoboken, New Jersey (2018)
- Tong, H.: Non Linear Time Series: A Dynamical System Approach. Clarendon Press, Oxford, England (1990)
- Vogel, C.R.: Computational Methods for Inverse Problems. SIAM Classics in Applied Mathematics, vol. 29. SIAM, Philadelphia, Pennsylvania (2002)
- Wooldridge, J.M.: Econometric Analysis of Cross Section and Panel Data, 2nd edn. The MIT Press, Cambridge, MA, USA (2010)